Technische Universität Wien

Institut für Analysis und Scientific Computing

Intracortical and Uniform E-field Stimulation of a Martinotti cell: A Computational Approach

DIPLOMARBEIT

von

Lydia Fani Simantiraki

ausgeführt zum Zwecke der Erlangung des akademischen Grades der

Diplom-Ingenieurin

im Rahmen des Studiums

Biomedical Engineering

eingereicht an der

Technischen Universität Wien

Betreuer: Univ. Prof. Dr.sc.med. Dr.techn. Dr.rer.nat. **Frank Rattay**

Wien, 2022

Vienna University of Technology

Institute of Analysis and Scientific Computing

Intracortical and Uniform E-field Stimulation of a Martinotti cell: A Computational Approach

MASTER THESIS

by

Lydia Fani Simantiraki

submitted in partial fulfillment of the requirements for the degree of

Master of Sciences

in

Biomedical Engineering

to the

Vienna University of Technology

Advisor: Univ. Prof. Dr.sc.med. Dr.techn. Dr.rer.nat. **Frank Rattay**

Vienna, 2022

στους γονείς μου

Kurzfassung

Das Ziel der vorliegenden Diplomarbeit ist die Implementierung von Rechenmodellen, die die Erregbarkeit einer Martinotti-Zelle durch Stimulation untersuchen. Die Zelle wurde als ein einfaches, lineares Neuron mit sphärischem Zellkörper (das Soma) modelliert und zusätzlich als ein dreidimensionales Neuron mit mehreren Abzweigungen, das einer echten Geometrie ähnelt.

Die Reaktion dieser Modelle wurde auf Stimulationen des intrazellulären, extrazellulären und homogenen elektrischen Feldes geprüft. Letzteres wurde für die Simulation der transkranialen Magnetstimulation verwendet.

Das Axonterminal war der Zellfortsatz mit der kleinsten Schwellenamplitude während der intrazellulären Stimulation. Während der extrazellulären kathodischen Stimulation wurden in ähnlicher Weise die weniger negativen Schwellenamplituden sowohl über dem Axonterminal des linearen Modells als auch über einer morphologischen Diskontinuität des dreidimensionalen Modells beobachtet.

Die transkraniale magnetische Stimulation verursachte in den meisten Fällen eine Auslösung des Aktionspotentials entweder an den Axonterminalen oder an den tatsächlichen Terminationsstellen. Sowohl für das lineare als auch für das dreidimensionale Modell wurden die Aktionspotentiale weder am Soma noch an den Initialsegmenten des Axons für keine der getesteten Orientierungen ausgelöst.

Abstract

The aim of this thesis is the implementation of computational models for the investigation of the excitability of a Martinotti cell upon stimulation. The cell was modeled as a simple, stick neuron with a spherical cell body (soma) and additionally as a three-dimensional neuron with several branches, resembling a real geometry.

The response of these models was tested to internal, external and uniform E-field stimulation. The latter was used for simulating transcranial magnetic stimulation.

The axon terminal was the process with the smallest threshold amplitude during intracellular stimulation. Similarly, during extracellular cathodic stimulation, the less negative threshold amplitudes were observed above the axon terminal of the linear model and above a morphological discontinuity of the three-dimensional model.

During transcranial magnetic stimulation the site of action potential initiation was the axon terminals or sites of termination in most of the cases. Spikes were not initiated at the soma or the axon initial segments for any orientation tested for both the linear and the three-dimensional models.

Acknowledgements

First I want to thank Professor Rattay for being the advisor of this thesis and for introducing me to Computational Neuroscience. I am extremely grateful for his support, guidance and always insightful feedback.

I would also like to thank Dr. Markus Hilscher for providing his overall input on Martinotti cells and for his valuable comments on this work.

I am thankful to my parents Vasiliki and Nikolaos for their unconditional love, encouragement and sacrifices; for always giving me the space and freedom to pursue my goals. And to my sister Katerina for always being by my side and whose support has always been precious. Finally to my grandparents Pinelopi and Xenophon for their limitless love, as well as to my uncles Ioannis and Georgios for the long and fruitful discussions.

I especially express my thankfulness to my partner Konstantinos Gavriil for his love and support all these years. His attitude and approach toward life and science have been inspiring to me. And of course I thank our amazing dog Pixel who kept me mentally balanced!

λφσ

Contents

Glossary **xv**

1 Introduction **1**
1.1 Motivation . . . 1
1.2 Cerebral Cortex . . . 1
1.3 Pyramidal Cells . . . 2
1.4 Martinotti Cells . . . 2
1.5 Somatostatin-expressing neurons . . . 4
1.6 Transcranial Magnetic Stimulation . . . 5

2 Neuronal Cells **9**
2.1 Neuron Properties . . . 9
2.1.1 Overview . . . 9
2.1.2 Structure . . . 10
2.1.3 Communication . . . 11
2.1.4 Cell Membrane . . . 12
2.1.5 Ion Channels . . . 15
2.1.6 Electrical Activity . . . 16
2.2 Electrophysiological Techniques . . . 20
2.2.1 The Voltage Clamp Technique . . . 20
2.2.2 The Current Clamp Technique . . . 21
2.2.3 The Patch Clamp Technique . . . 21

3 Mathematical Description **23**
3.1 Cable Theory . . . 23

3.2 Membrane Models . . . 24
3.2.1 Neuron as an RC circuit . . . 24
3.2.2 HH type models . . . 33
3.3 Compartment Modeling . . . 33
3.4 Electrical Stimulation . . . 36
3.4.1 Influence of extracellular potential . . . 37

4 Modeling a Martinotti Cell **43**
4.1 Implementation Details . . . 43
4.1.1 NEURON . . . 43
4.1.2 Single Compartment Model . . . 44
4.2 Multicompartment Model . . . 46
4.2.1 Linear Model . . . 47
4.2.2 3D Model . . . 53

5 Results **59**
5.1 Simulation Details . . . 59
5.1.1 Electrical Stimulation . . . 59
5.1.2 Transcranial Magnetic Stimulation . . . 60
5.2 Single Compartment Model . . . 61
5.3 Multicompartment Models . . . 62
5.3.1 Intracellular vs Extracellular Stimulation . . . 62
5.3.2 Transcranial Magnetic Stimulation . . . 74

6 Conclusion **85**
6.1 Limitations . . . 86

Bibliography **87**

Glossary

ρ_i	Intracellular resistivity.
ρ_e	Extracellular resistivity.
c_m	Specific membrane capacitance.
g_K	Maximum potassium conductance.
g_{leak}	Leakage conductance.
g_M	Maximum conductance of M current.
g_{Na}	Maximum sodium conductance. $g_{Na_v1.2}$, $g_{Na_v1.6}$ are the maximum conductances of the fast threshold $Na_v1.2$ and low threshold $Na_v1.6$ sodium channels respectively.
g_T	Maximum conductance of T current.
i	Current density.
k	Temperature coefficient.
F	Faraday's constant.
GABA	The main inhibitory neurotransmitter in the body.

$GABA_A$	GABA receptor with a ligand-gated chloride channel that mediates fast inhibitory signals through rapid postsynaptic membrane hyperpolarization.
$GABA_B$	GABA receptor that produces slow and prolonged inhibitory signals.
$I_{electrode}$	Electrode current.
$I_{stimulus}$	Injected current.
R_a	Axial (cytoplasmic) resistivity in NEURON.
V	Reduced membrane potential (0 in resting state).
V_e	Extracellular potential.
V_i	Intracellular potential.
V_{rest}	Resting potential.

Chapter 1

Introduction

1.1 Motivation

Electrical stimulation is a strategy for modulating the nervous system by taking advantage of the mechanism of neural signaling. It is used for pain relief, rehabilitation reasons and for the improvement of mobility after injuries.

Transcranial magnetic stimulation (TMS) affects the action of feedback projections leading to a disruption in perception. It is widely used to investigate complex facets of the human brain, including sensory and motor function, as well as cognition.

TMS of Martinotti cells can potentially help in the treatment of various pathologies and diseases, especially because of the short distance of magnetically induced stimulation effects. Martinotti cells are neurons in the main cortical output layer V, with most of their axons projecting to layer I of the cortex. They are responsible for providing a frequency-dependent disynaptic inhibition on neighboring pyramidal cells.

1.2 Cerebral Cortex

The human cerebral cortex has six layers (neocortex) and contains approximately 21 to 26 billion neurons [39]. Most of the neurons in the cerebral cortex are arranged vertically and most abundant neurons are the efferent pyramidal cells [55]. The first

layer (I) is the most superficial and consists only of a few nerve cells; the outer granular layer (II) is a relatively thin one, consisting of numerous small and densely packed neurons. Layer III is composed of medium-sized pyramidal nerve cells. Layer IV contains small, irregularly shaped nerve cells, whereas layer V includes large pyramidal cells. The 6th layer (VI) consists of small polymorphic and fusiform nerve cells, as shown in Figure 1.1.

There are two dominant families of neurons in the cortex; excitatory neurons release the neurotransmitter glutamate and depolarize the postsynaptic neuron. Inhibitory neurons release γ-amino-butyric acid (GABA) and they play a critical role in a variety of pathophysiological processes, such as in the modulation of cortical and hippocampal neural circuitry and activity, cognitive function-related neural oscillations and information integration and processing [64].

1.3 Pyramidal Cells

Pyramidal cells are distinguished by their distinct apical dendrite and basal dendritic tree, including an apical tuft, and the pyramidal shape of their soma. They are found in several regions of the CNS, comprising approximately 70–90% of all neurons in cortex. Their plethora places them center-stage for many important cognitive processes, as they generate nearly all cortically initiated excitation [13]. They are necessary for the processing of external signals and motor control.

1.4 Martinotti Cells

Martinotti cells (MC) mostly display ovoid somata and bitufted dendrites, with their axon often emerging from the "main" dendrite, branching close to the soma and ascending to the first cortical layer. Additional feature is that the dendritic tree is significantly smaller than the axonal tree. Their ubiquitous existence in different layers of the cerebral cortex of different ages and species suggests a central role in information processing in the cortical column. They are generally considered low-threshold, regular spiking interneurons.

This type of interneurons has been proposed to be involved in memory forma-

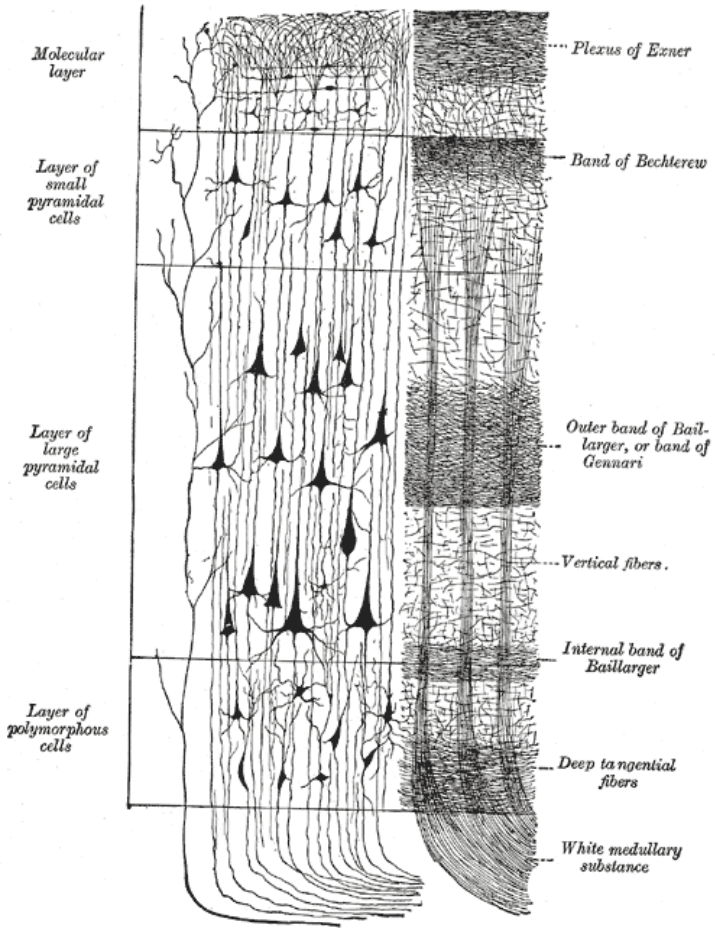

Figure 1.1: The layers of the cerebral cortex shown in Gray's Anatomy book [21].

tion and storage, as well as in neurodegenerative diseases [15]. They are crucial for feedback inhibition in and between neocortical layers and columns [63].

The function of Martinotti cells arises from their interaction with layer V pyramidal cell dendrite, onto which they make functional GABAergic synapses. They send axons to layer I in the cortex to contact and inhibit the dendritic tufts of pyramidal cells. Their axons can spread horizontally in layer I for several millimeters and therefore provide synaptic inhibition across cortical columns [18].

More specifically, L5 Martinotti cells provide a frequency-dependent disynaptic inhibition (FDDI) on neighboring pyramidal cells, an inhibitory mechanism where two or more pyramidal cells synchronize via one or a few intermediate Martinotti cells. As reported in [53], there is a disynaptic inhibitory pathway among neocortical pyramidal cells which is mediated by Martinotti cells (Figure 1.2). Martinotti cells receive facilitating excitatory synapses from a pyramidal cell and in turn form inhibitory synapses (depressing GABAergic input) onto neighboring pyramidal apical and tufted dendrites. FDDI can be triggered by a brief, high frequency burst in the presynaptic pyramidal cell. Repetitive activation of Martinotti cells causes brief and small hyperpolarizing potentials in the pyramidal cell dendrites, inactivating the calcium spike initiation zone of pyramidal cells via $GABA_A$-mediated dendritic inhibition [38].

Such a reliable activation of inhibitory pathway is crucial for a normal activity in the cortex, as imbalances are linked to pathologies such as epilepsy [9].

The most frequently used genetic marker to identify them is somatostatin. As stated in [23], Chrna2 is a highly specific marker for L5 Martinotti cells that project to the first layer, and Chrna2-expressing MC only target a specific subtype of pyramidal cells, the thick-tufted of layer V. Moreover, the mechanism of Martinotti cell inhibition, which is frequency dependent, can initiate and maintain synchronous firing between pyramidal cells.

1.5 Somatostatin-expressing neurons

Somatostatin-expressing neurons (SST) are a subset of GABAergic interneurons, including the Martinotti cells. In general, this type of cells has a low threshold for action potential generation and often classified as low-threshold spiking cells. They are

connected to nearby pyramidal cells, forming local networks and regulating the local neural activity and they serve as source of inhibition in to many different cell types in the neocortex.

When these neurons release GABA, it activates presynaptic $GABA_B$ receptors on pyramidal cells and silences connections between pyramidal neurons. The high connection probability between SST and pyramidal neurons, suggests that SST cells could provide precisely timed feedback inhibition of local pyramidal neurons through Martinotti cells [59].

Although it was believed that they only have a role in fast $GABA_A$-mediated inhibition, by providing fast synaptic input onto the distal pyramidal dendrites spontaneous activity of these interneurons can also mediate presynaptic $GABA_B$ activation. As reported in [60] they are able to silence excitatory synaptic connections through the regulation of presynaptic release in a rapid and reversible manner.

1.6 Transcranial Magnetic Stimulation

Transcranial magnetic stimulation uses the principle of Faraday's electromagnetic induction to noninvasively stimulate muscles or nerves for diagnostic and therapeutic purposes, such as alleviation of symptoms of schizophrenia and depression [17].

Anthony Barker was the first to start a research on using time-varying magnetic fields to induce current flow in tissue in order to depolarize neurons. Prior to this, the alternative was direct electrical stimulation, with electrodes placed on the scalp, a method that is often painful.

TMS generates a brief, high-intensity magnetic field by passing a brief electric current through a magnetic coil that is placed over a subject's head, affecting the brain activity in an awake alert human. The magnetic pulse penetrates the scalp and skull to reach the cortex and in turn induces a secondary ionic current in the brain which can trigger action potentials in superficial cortical neurons (Figure 1.3). Short (approximately $200-500\,\mu s$), but strong ($> 1.5\,T$) bursts of TMS can effectively perturb the ongoing neural processing, by producing synchronized activation of cortical neurons, followed by inhibition [33].

According to [37] on experiments in L5 pyramidal neurons, TMS leads to suppression of dendritic Ca^{2+} activity, by first activating dendrite-targeting inhibitory neu-

rons. The inhibition results due to the recruitment of cortical interneurons mediating both $GABA_A$ and $GABA_B$-receptor-activated inhibition in the pyramidal dendrites. L5 pyramidal dendrites are strongly inhibited by activation of $GABA_A$ and post-synaptic $GABA_B$ receptors.

It is worth mentioning that there is no single, universally effective electric field strength value, despite standardization of the electric field strength. It is likely, that different neural effects are induced by different electric field strengths [58]. Another important characteristic is that the electric field estimation can only provide approximate values of the actual electric field produced.

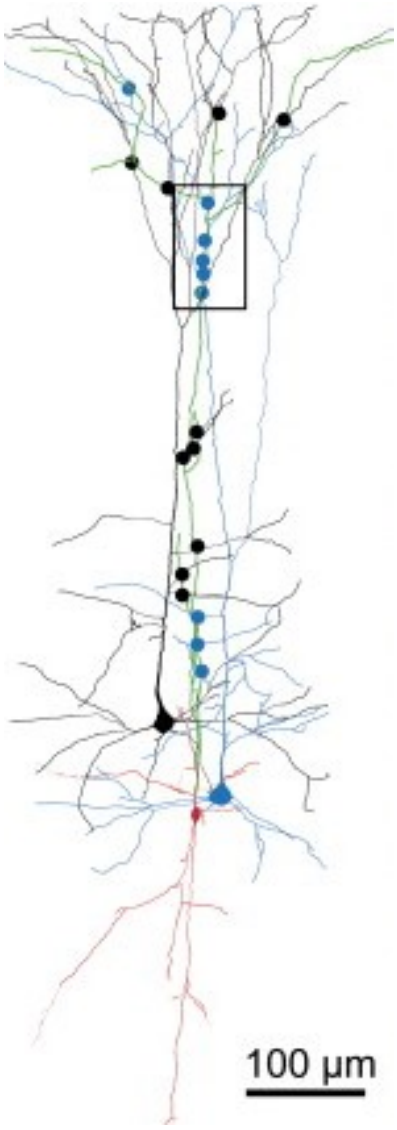

Figure 1.2: Martinotti cells (soma, dendrites in red, axons in green) mediate disynaptic inhibition between neocortical pyramidal cells (somata, dendrites in black and blue). The filled circles indicate the synapses with the targeted pyramidal dendrite [[53]].

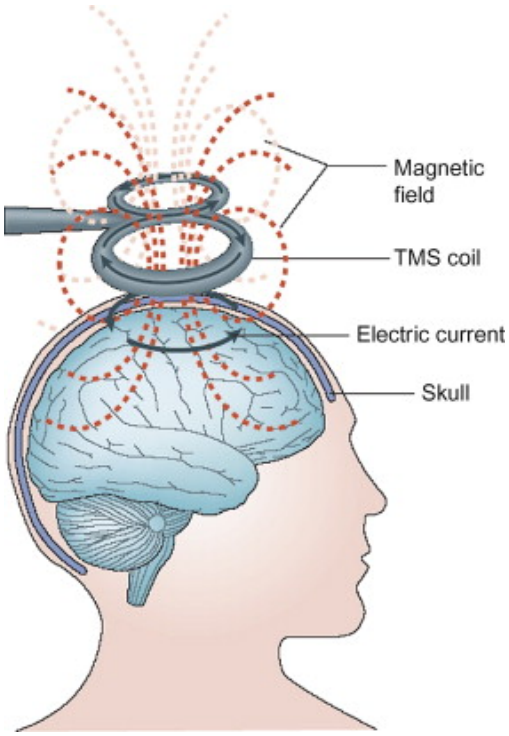

Figure 1.3: Induction of electrical currents in the brain through the magnetic pulses (dashed lines) during TMS [54].

Chapter 2

Neuronal Cells

2.1 Neuron Properties

2.1.1 Overview

Neurons are the fundamental units of the nervous system; their electrical activity enables them to perform their prestigious task of signal generation and transmission.

Based on their functionality there are three types of neuronal cells: the motor neurons, the sensory neurons and the interneurons; the latter are exclusively found in the central nervous system. Neurons that develop from cells within the spinal cord are called motor, whereas those that develop from neural crest cells are sensory neurons.

Somatic sensory neurons carry information from the periphery into the central nervous system (brain and spinal cord), and are also called somatic sensory afferents. Somatic motor fibers carry information away from the central nervous system to skeletal muscles and are also called somatic motor efferents. Interneurons transfer signals between sensory and motor neurons, being able to communicate with each other, forming circuits of various complexity.

The structural neuron classification is based on the number of processes that extend from the soma. The major classification is multipolar, bipolar, and unipolar neurons (Figure 2.1). Multipolar neurons have three or more processes that extend out from the cell body. Another category is the so called pseudounipolar neurons which start out during development as bipolar neurons with a central process ex-

tending into the spinal or trigeminal dorsal horn, and a peripheral process extending out to peripheral targets.

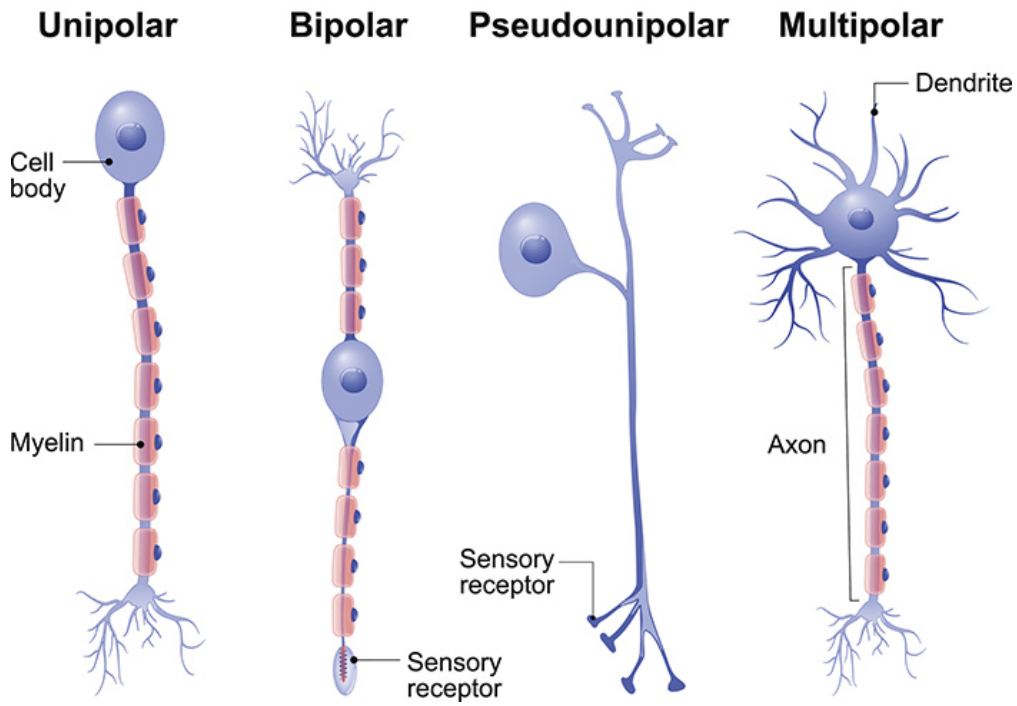

Figure 2.1: Structural classification of neurons [41].

2.1.2 Structure

Nerve cells consist of the soma, the cell body that includes the nucleus and two kinds of processes: the dendrite and the axon (nerve fiber), as seen in Figure 2.2. The dendritic and axonal processes may have ramifications, resulting in dendritic and axonal branches.

Dendrites receive the signals and then convey them toward the soma by changing the electrical polarization of the cell membrane. If this change is strong enough that causes a suprathreshold potential, an action potential is generated and propagated down the axon.

The axon can be very long and often myelinated. Myelinated axons are completely covered by myelin sheaths (internodes), except at the small gaps that are called nodes of Ranvier and are directly exposed to the extracellular milieu. The

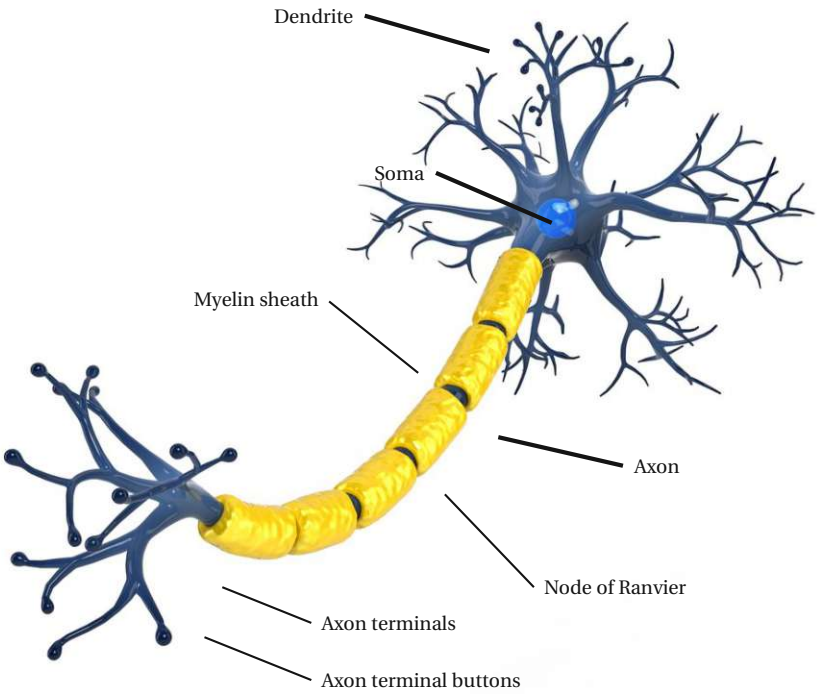

Figure 2.2: Major parts of a neuron [14].

myelin sheath consists of several layers of glial cell membrane and works as an electrical insulator. When the membrane at the node is excited, the local circuit generated cannot flow through the high-resistance sheath and therefore, flows out through and depolarizes the membrane at the next node. The low capacitance of the sheath results in small energy requirement in order to depolarize the remaining membrane between the nodes, which leads to local circuit spreading at an increased speed. Active excitation of the axonal membrane jumps from node to node, a form of impulse propagation that is called saltatory conduction. Such movement of the wave of depolarization is much more rapid than in unmyelinated fibers.

2.1.3 Communication

Different neurons form synapses with each other in order to communicate. These are points at which an impulse is transmitted from one nerve cell, the 'presynaptic' neuron, onto a dendrite or cell body of another one, the 'postsynaptic' neuron, at a narrow gap between the neurons, known as a gap junction.

Some signalling is purely electrical, where transmission occurs via electrical coupling of ion movements at gap junctions. Electrical synapses thus work by allowing ionic current to flow passively through the gap junction pores from one neuron to another, with the usual source of this current being the potential difference generated locally by the action potential.

However, most transmissions usually involve a chemical step; the chemicals that mediate synaptic transmission are called neurotransmitters, as seen in Figure 2.3. The process is initiated when an action potential invades the terminal of the presynaptic neuron, which changes the membrane potential. This leads to the opening of voltage-gated calcium channels in the presynaptic membrane. The opening of these channels causes a rapid influx of Ca2+ into the presynaptic terminal, which results in elevation of the presynaptic Ca2+ concentration of the cytoplasm in the terminal. This allows synaptic vesicles to fuse with the plasma membrane of the presynaptic neuron. Transmitters are released and then diffuse across the synaptic cleft, binding to specific receptors on the membrane of the postsynaptic neuron. The binding of neurotransmitter to the receptors causes channels in the postsynaptic membrane to open (or sometimes to close), thus changing the ability of ions to flow into (or out of) the postsynaptic cells. The resulting neurotransmitter-induced current flow alters the conductance and usually the membrane potential of the postsynaptic neuron, increasing or decreasing the probability that the neuron will fire an action potential [12].

In that sense, neurons are divided into two kinds: excitatory and inhibitory. In the first one, the presynaptic neuron activates the postsynaptic neurons, whereas in the second kind, the signal of the presynaptic neuron either diminishes or suppresses the activity of the postsynaptic neuron. Individual neurons receive usually both excitatory and inhibitory synapses.

2.1.4 Cell Membrane

The membrane of the neuron is composed of two layers of lipids, as seen in Figure 2.4. These fundamental blocks, the phospholipids are amphipathic molecules, consist of two hydrophobic fatty acid chains linked to a phosphate-containing hydrophilic head group. Because their fatty acid tails are poorly soluble in water, phos-

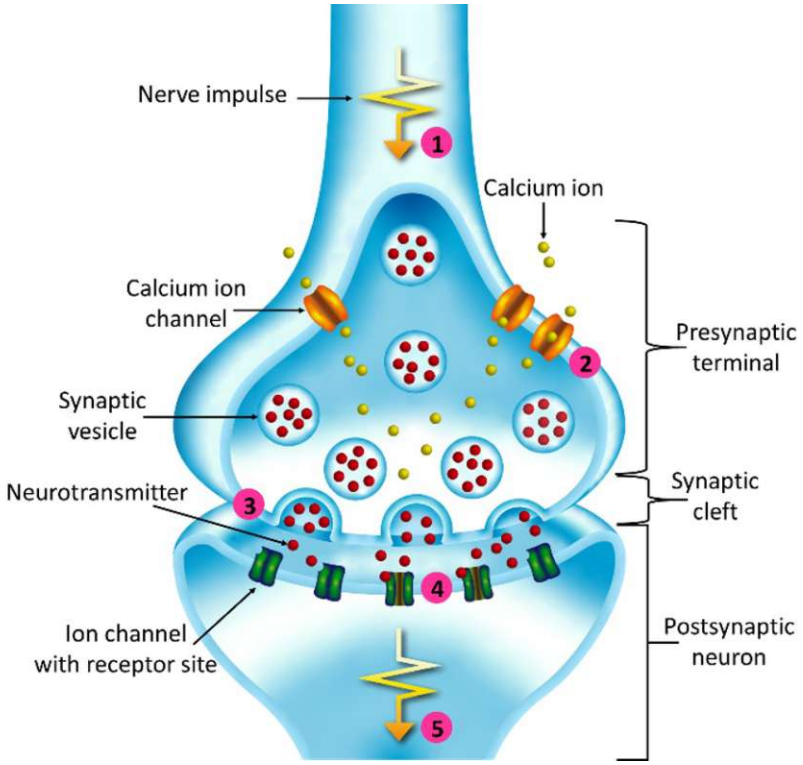

Figure 2.3: A chemical synapse [57].

pholipids spontaneously form bilayers in aqueous solutions. Their hydrophobic tails are buried in the interior of the membrane and the polar head groups are exposed on both sides, in contact with water. One tail usually has one or more cis-double bonds, each of creating a small kink in the tail while the other tail does not. The double bond means that the fatty acid is unsaturated, while the single bond indicates saturation.

Such phospholipid bilayers form a stable barrier between two aqueous compartments, keeping outside molecules from entering the cell and represent the basic structure of all biological membranes.

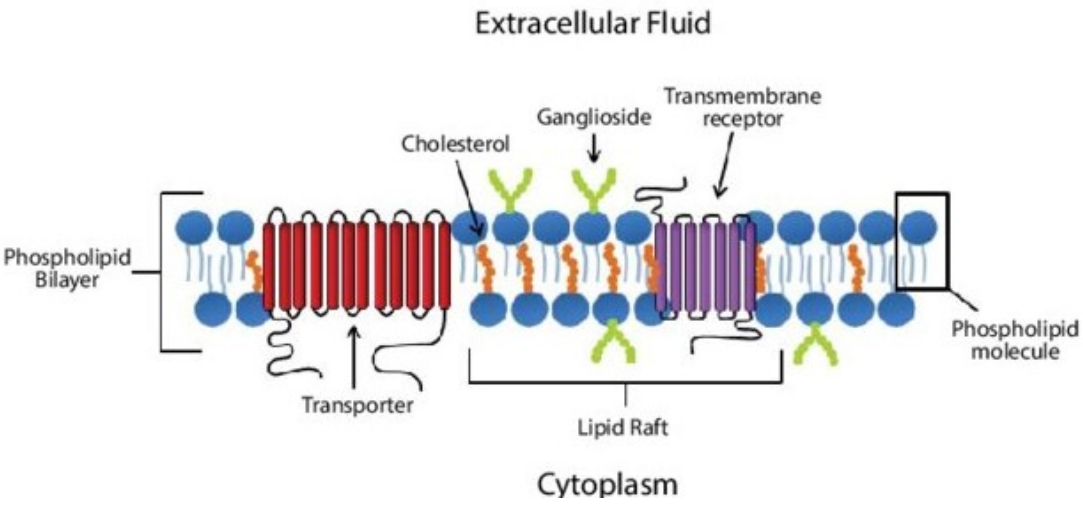

Figure 2.4: The cell membrane consists of lipids and embedded proteins. Each phospholipid is made up of two fatty acids, a phosphate group amd a glycerol molecule [7].

An important property of lipid bilayers is that they behave as two-dimensional fluids in which individual molecules are free to rotate and move in lateral directions, a critical property of membranes.

The other major constituent of cell membranes is the proteins which are inserted into the lipid bilayer. While phospholipids provide the basic structural organization of membranes, membrane proteins carry out the specific functions of the different membranes of the cell.

Regarding the permeability of phospholipid bilayers, only small uncharged molecules can diffuse freely through them. Small nonpolar molecules, such as O2 and CO2, are soluble in the lipid bilayer and therefore can readily cross cell membranes, whereas small uncharged polar molecules, such as H2O, also can diffuse through membranes.

However, the bilayer is impermeable to larger uncharged polar molecules, such as glucose and amino acids, or charged molecules, such as ions [11].

Molecules that cannot diffuse across the lipid bilayer, pass across membranes via the action of specific transmembrane proteins, which act as transporters. This passage allows polar or charged molecules to cross the membrane through a protein pore without interacting with the hydrophobic fatty acid chains of the membrane phospholipids.

There are two general classes of membrane transport proteins. Channel proteins form open pores through the membrane, allowing the free passage of any molecule of the appropriate size at a fast rate. On the other hand, carrier proteins selectively bind and transport specific small molecules, such as glucose. They act like enzymes to facilitate the passage of specific molecules across membranes, by binding specific molecules and then undergo conformational changes that open channels through which the molecule to be transported can pass across the membrane and be released on the other side. Carrier proteins are classified as active or passive, depending on whether the translocated molecules are moved up or down their electrochemical gradients, respectively.

Molecules transported by either channel or carrier proteins cross membranes in the energetically favorable direction, as determined by concentration and electrochemical gradients, that is passive transport.

Another important protein, the sodium potassium pump is programed to pump two molecules of potassium into the cell for every three molecules of sodium out of the cell [31]. This maintains the internal concentration of potassium ions K^+ higher than that in the surrounding medium and at the same time the internal concentration of sodium ions Na^+ lower than that of the surrounding medium. The pump has adenosine-triphosphatase (ATPase) activity since it moves the ions against their concentration gradients and by maintaining the difference in concentrations of Na^+ and K^+ is responsible for the resting potential of cells.

2.1.5 Ion Channels

The specialized proteins in the plasma membrane that provide a passageway through which charged ions can cross the plasma membrane down their electrochemical gra-

dient are called ion channels. Once open, channel proteins form small pores through which ions of the appropriate size and charge can cross the membrane by free diffusion. The pores formed by these channel proteins are not permanently open. On the contrary, they have specificity filters at their entrance, which makes them be selectively opened and closed in response to extracellular signals, allowing the cell to control the movement of ions across the membrane. As ion concentrations are increased, the flux of ions through a channel increases proportionally but then levels off (saturates) at a maximum rate [2].

The gate opens in response to a specific triggering stimulus that causes the transition from resting to open through the process of activation. The main types of stimuli that are known to cause ion channels to open are a change in the voltage across the membrane (voltage-gated channels), a mechanical stress (mechanically gated channels), or the binding of a ligand (ligand-gated channels). Voltage-gated ion channels have three primary conformational states: resting and inactivated closed states, and an open conducting state, and are responsible for the production of action potentials. In contrast, ligand-gated ion channels are activated by ligands (such as a neurotransmitter) binding to an extracellular receptor site and they also have resting and open states [19]. They are responsible for the generation of graded potentials.

2.1.6 Electrical Activity

Membrane Potential

The cell membrane is surrounded by extracellular fluid on its outer side and cytoplasm on its inner side. The ionic concentration of these two differs greatly, a fact that results in a constant transfer of ions across the membrane. This transfer of electrically charged ions generates tiny voltage potentials, called membrane potentials.

At rest, the neuron is in a slightly polarized state, meaning that the electrical charge across the membrane is about -70 mV. At this state the neuron is said to be at its resting membrane potential. This is because the interior of the neuron (cytoplasm) has an excess of negative charge, mainly contributed by cytoplasmic proteins and other macromolecules inside the cell (potassium ions K^+ also play a significant role in electrical activity), whereas the exterior has a positive charge, contributed by the sodium ions Na^+ in the extracellular fluid.

Even at rest the cell membrane is 'leaky' to some extent, and therefore there is a tendency for this system to achieve a state of equilibrium when the transfer of ions comes to a standstill. However, neurons, in order to be in an excitable state, must be in a polarized, because a state of equilibrium does not generate any potential.

The reversal potential (also called Nernst or equilibrium potential) of a specific ion is the membrane potential at which there is no net flow of the ion from one side of the membrane to the other. This means, that the equilibrium potential is the voltage which exactly balances the ion flux. This electrical potential difference is based on the Nernst equation:

$$E_{\mathrm{m}} = \frac{RT}{zF} ln \frac{c_{\mathrm{e}}}{c_{\mathrm{i}}} \tag{2.1}$$

where $R = 8.31441\ \mathrm{J\,mol^{-1}\,K^{-1}}$ is the gas constant, T is the temperature in kelvin, z is the valence and F is the Faraday constant, representing the magnitude of electric charge per mole of electrons and has the value $F = 96485\ \mathrm{C\,mol^{-1}}$. The external and internal ion concentrations are c_{e} and c_{i} respectively.

The reversal potentials of the cations K^+ and Na^+ are about $E_{\mathrm{K}} = -90$ mV and $E_{\mathrm{Na}} = +55$ mV, and of the anion Cl^- is $E_{\mathrm{Cl^-}} = -50$ mV.

For a cell permeable to only one ionic species (only one type of ion that can cross the membrane), the resting membrane potential will equal the equilibrium potential for that ion.

When more than one ions are involved, the steady state membrane voltage E_{rest} is defined by the Goldman-Hodgkin-Katz equation, which has the following form when K^+, Na^+ and Cl^- ions are considered:

$$E_{\mathrm{m}} = \frac{RT}{F} ln \frac{P_{\mathrm{K}}[\mathrm{K}]_{\mathrm{e}} + P_{\mathrm{Na}}[\mathrm{Na}]_{\mathrm{e}} + P_{\mathrm{Cl}}[\mathrm{Cl}]_{\mathrm{i}}}{P_{\mathrm{K}}[\mathrm{K}]_{\mathrm{i}} + P_{\mathrm{Na}}[\mathrm{Na}]_{\mathrm{i}} + P_{\mathrm{Cl}}[\mathrm{Cl}]_{\mathrm{e}}} \tag{2.2}$$

where [K], [Na], [Cl] are the potassium, sodium and chloride concentrations respectively, and e, i stand for extracellular and intracellular. P_{K}, P_{Na}, P_{Cl} are the permeabilities in cm/ sec which refers to the ease with which ions cross the membrane.

At the resting state, the membrane is most permeable to potassium ions and thus the resting membrane voltage is close to the potassium Nernst potential, that is about −70 mV.

When neurons are excited the electrical properties of their membranes change,

resulting in the generation of different types of nerve signals.

If changes within the neuron increase the negative charge occurring at the resting state, the neuron is said to be in a hyperpolarized state, and getting the neuron to fire is more difficult. Hyperpolarization is determined by many factors, one of which is the flow of ions in and out of the cell.

Sodium channels cause influx (entry to inside) of Na^+ ions into the neurons which causes the negative charge inside it to decrease (because of the relative increase of positive charges inside), a phenomenon called depolarization. In a state of depolarization the neurons are excited and the signals between the neurons or across the nerves are allowed to pass. On the other hand, potassium channels cause efflux (exit to outside) of K^+ ions, resulting in an increase of negative charge inside the neuron (because of the relative decrease of positive charges inside), which is the above mentioned hyperpolarization. In a state of hyperpolarization the signals between the neurons or across the nerves are not passed, which means that the message is blocked.

Sometimes, the chloride channels cause an influx of Cl^- ions (increasing negative charges inside) into the neuron, which make the neuron hyperpolarized, decreasing its excitability, that means much more stimulation will be necessary to get it to fire.

Calcium channels also influence excitation indirectly. They carry a positive charge, and when membrane channels open they allow calcium to flow into the cell, that means a decrease in Ca^{2+} concentration in the extracellular fluid and firing becomes much more likely.

Electrical Properties

A membrane's electrical properties derive from fundamental physical laws and include the concepts of electrical current, potential or voltage, capacitance, and resistance.

Because the membrane impedes ion flow, it electrically insulates the intracellular and extracellular solutions, which themselves are excellent conductors because of their high ion concentrations. This arrangement results in significant membrane capacitance (C_m). Ions, penetrate the bilayer, resulting in a finite but large membrane resistance (R_m).

The electrical properties of the membrane can be represented by an equivalent circuit involving resistance and capacitance elements, as it will further be discussed in the next chapter. The voltage across this circuit is the membrane potential (V_m).

Action potential

Action potentials are large electric potentials generated during neuron excitation. The rapid and synchronized excitation of Na^+ and K^+ channels result in its generation.

An action potential is the result of sufficient electrical excitation, that causes the membrane voltage to reach a certain threshold, and it can either be generated fully or not at ll (all-or-none phenomenon). Once generated at the axon hillock, it 'travels' down the length of the axon in a manner analogous to the way that electricity travels across a wire until it reaches the terminal bulb, where contact is made with another neuron to which it passes the electrical signal.

During an action potential (Figure 2.5), first a large number of voltage-gated sodium channels open (opening of activation gate), allowing an inward rush of Na^+ into the cell, and the voltage reaches about −50 mV (threshold). This is the depolarizing phase and produces the ascending phase of the action potential. Then, once the peak excitation is reached, the repolarization phase that produces the descending phase starts by two mechanisms: by the inactivation of sodium channels (the inactivation gate closes at the peak), and by the activation of potassium channels, which drives K^+ out of the neuron, lessening the positive charge inside. During repolarization, no more sodium ions can enter the cell. At the end of an action potential, neurons are at a hyperpolarization phase. This happens because of continued efflux of K^+ ions making the inside charge even more negative; the voltage gated potassium channels close with a little delay. The membrane can return to the resting potential because of the ongoing activity of the non-gated channels and the sodium-potassium pump.

The refractory period is the time after an action potential is generated, during which the excitable cell cannot produce another action potential. There are two subphases of this period. The absolute refractory period, where an action potential cannot be generated, because all the voltage-gated sodium channels are already opened or being opened at their maximum speed. During the relative refractory period, the

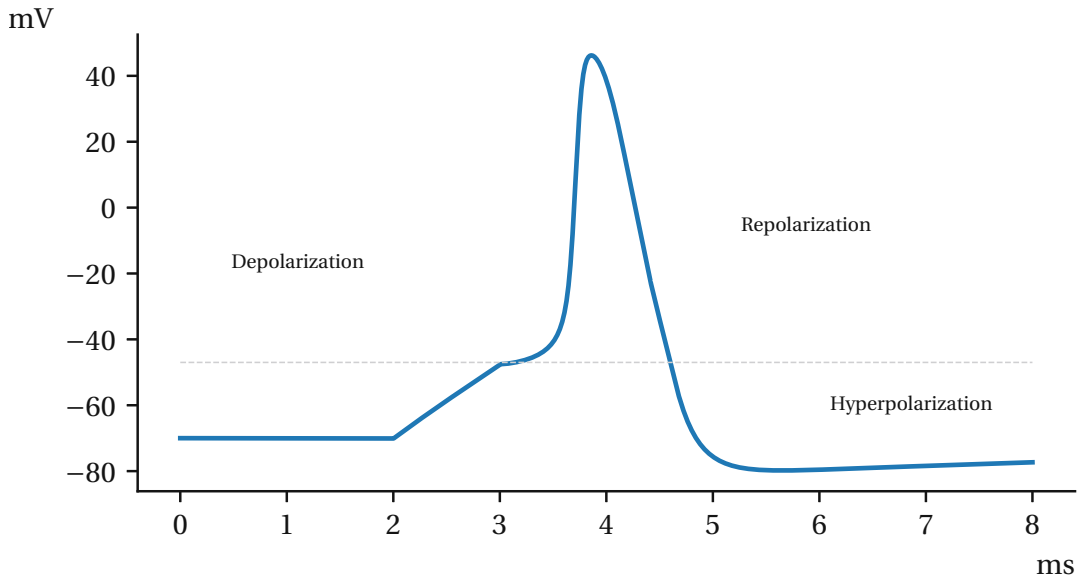

Figure 2.5: An action potential is generated after the membrane potential exceeds a certain threshold (grey dashed line).

generation of a new action potential is possible, but only upon a suprathreshold stimulus.

2.2 Electrophysiological Techniques

2.2.1 The Voltage Clamp Technique

The voltage clamp constitutes a classic technique for measuring ionic currents across the cell membrane. By setting a desired membrane potential, the required currents are injected through an electrode in order counteract any changes to that voltage, and then measured.

The voltage clamp device uses a negative feedback circuit to control the membrane voltage. This is accomplished by using two microelectrodes inserted into the cell, one for measuring the voltage and the other for the current injection.

2.2.2 The Current Clamp Technique

In current clamp recording, the current, instead of the voltage is clamped, monitoring the changes in the membrane voltage. This type of experiment mimics the current produced by a synaptic input.

2.2.3 The Patch Clamp Technique

The patch clamp technique is the basis of modern electrophysiology, allowing the investigation of a small set or even single ion channels [22].

The idea of G. Marmont and K. Cole was to eliminate space as variable and the voltage gradients along the axon.

A glass micropipette is tightly sealed onto the cell membrane, electrically isolating a small membrane patch. Currents fluxing through the channels in this patch can flow into the pipette and can be recorded by an electrode that is connected to a highly sensitive differential amplifier (Figure 2.6).

In the voltage clamp configuration, a current is injected into the cell via a negative feedback loop to compensate changes in membrane potential. Recording this current allows conclusions about the membrane conductance.

Current clamp can also be used to measure changes in membrane voltage. Voltage or current change within cell membranes can be altered by applying compounds to block or open channels.

The advances of this method is the increased control of the membrane potential, the study of isolated membrane patches, as well as the dramatically decreased electrical noise.

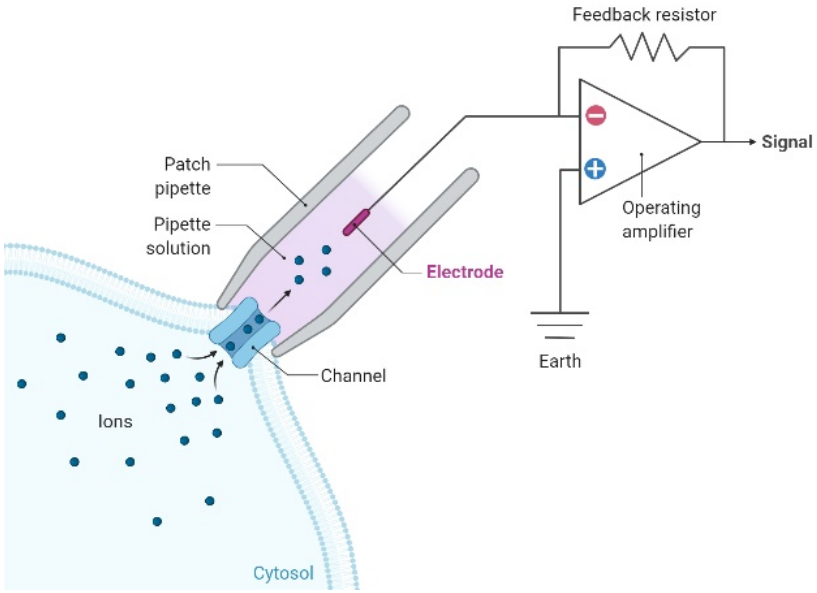

Figure 2.6: The patch clamp recording principle: mild suction is applied to gain a seal between the pipette and the membrane. The currents are recorded by the electrode attached to the amplifier [3].

Chapter 3

Mathematical Description

3.1 Cable Theory

Wilfrid Rall introduced the cable theory for neurons, providing a general mathematical modeling framework of spatio-temporal voltage dynamics in dendrites [[42], [43]].

Based on the simplification that current and voltage only depend on the length x of the process, the dendrite is subdivided into pieces of equal length Δx. Each piece can be simulated as a 'local model', where the extracellular medium is either inexistent or modeled as a resistor.

The resistance between two points along the conductor increases proportionally to their distance. In contrast, the transmembrane conductance (and capacity) of the membrane between the two points decreases with their distance.

The transmembrane current per unit length i_m will be the sum of the capacitive and passive ('leak') current:

$$i_m = -\frac{\partial(i_\mathrm{i} - i_\mathrm{e})}{\partial x} = c_m \frac{\partial(V_\mathrm{e} - V_\mathrm{i})}{\partial t} + \frac{V_\mathrm{e} - V_\mathrm{i}}{r_m} \tag{3.1}$$

From where we get:

$$\frac{r_m}{r_\mathrm{i} + r_\mathrm{e}} \frac{\partial^2 V_m}{\partial x^2} = r_m c_m \frac{\partial V_m}{\partial t} + V_m \tag{3.2}$$

and if we assume $r_\mathrm{e} = 0$, and divide by the membrane resistance per unit r_m, the

cable equation has the form:

$$\frac{1}{r_i}\frac{\partial^2 V_m}{\partial x^2} = c_m\frac{\partial V_m}{\partial t} + g_m V_m \tag{3.3}$$

where $g_m = \frac{1}{r_m}$, the membrane conductance per unit length.

3.2 Membrane Models

3.2.1 Neuron as an RC circuit

As mentioned in the previous chapter, the passive electrical properties of a neuron's cell membrane can be modeled as an electrical *RC* circuit (Figure 3.1), in order to calculate its membrane potential.

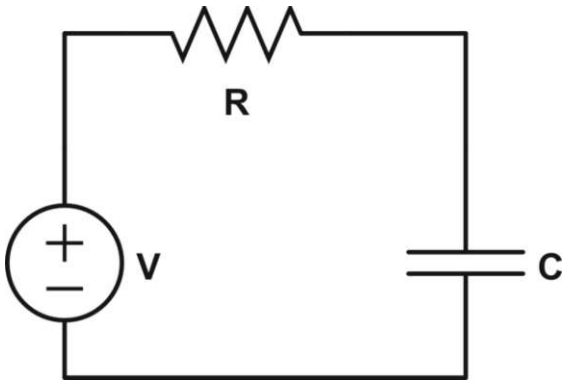

Figure 3.1: A simple *RC* circuit, composed of the passive components of a resistor *R* and a capacitor *C*.

The membrane of a neuron is often related to a capacitor because of its ability to store and separate a charge. In an electrical circuit, a capacitor possesses two conducting regions (conducting plates) with a separation of non-conducting material in between (dielectric). When one conducting region accumulates a charge, an electric field is created, which pushes the charge off of the subsequent conducting region of the capacitor. This phenomenon only lasts a short amount of time, producing a brief current. In a neuron, the conducting regions of the capacitor are represented by the conductive intracellular and extracellular solutions of the cell. The non-conducting insulator of the capacitor represents the non-conducting membrane of the neuron.

Ion channels allow current to flow in and out of the cell. When more ion channels are open, more ions are able to flow. This represents a decreased resistance, which leads to an increase in conductance.

As passive transports, ion channels can be represented with resistors in an RC circuit. Membrane resistance is highly nonlinear because of the activity of the ionic channels embedded in the membrane. The amount of current flowing through these resistors can be expressed by Ohm's Law (Equation 3.4).

The concentration gradient of a neuron is the external to internal ratio of ion concentration, and can be represented as a battery in the circuit. The battery symbolizes the overall differences in ion concentration inside and outside of the cell (more positive and more negative) that generate voltage [[30]].

From Ohm's law we get that the resistance in Ω will be:

$$R = \frac{V}{I_R} \tag{3.4}$$

where I_R is the resistor current and in terms of conductance $g = \frac{1}{R}$. The capacitance in F is given by the formula:

$$C = \frac{Q}{V} \tag{3.5}$$

where Q is the charge in Coulombs. This gives us that the voltage across the capacitor is $V = \frac{Q}{C}$, and the change of voltage in the capacitor will be:

$$\Delta V = \frac{\Delta Q}{C} \tag{3.6}$$

However, the capacitance current is I_C is:

$$I_C = \frac{\Delta Q}{\Delta t} \tag{3.7}$$

The total current will be the sum of I_R and I_C.

Passive Model

Based on the cable theory, a neuron can be modeled with its passive properties.

The passive model represents the passive properties of a cell membrane, meaning

that the resistor only represents the leakage current.

When an injecting current I_{stimulus} is applied intracellularly, the membrane current is used to load the capacitor and the resistor, and thus divided into a capacitive current and an ionic current $I_{\text{stimulus}} = I_R + I_C$:

$$I_{\text{stimulus}} = C_{\text{m}} \frac{dV}{dt} + I_{\text{ion}} \tag{3.8}$$

so the rate of the membrane voltage change is:

$$\frac{dV}{dt} = (-I_{\text{ion}} + I_{\text{stimulus}}) / C_{\text{m}} \tag{3.9}$$

Assuming an inside potential V_{i} and an external potential V_{e}, the voltage will be $V = V_{\text{i}} - V_{\text{e}} - V_{\text{rest}}$ across the membrane.

The time constant of the membrane defines how quickly the transient behavior returns to the steady state: $\tau = RC$

Integrate and Fire Model

The integrate and fire model is a simplified model and one of the most widely used for analyzing how a neural system behaves in terms of the injected current it receives.

This model captures the idea that a neuron spends most of its time integrating its inputs and making decisions on when to spike. The spikes are discrete, stochastic events described by the Poisson process, and occur when the voltage reaches the spike threshold. What is calculated is the rate a neuron fires as a function of how much input a cell gets. When a step current is injected, the neuron generates spikes at regular intervals, with these intervals being controlled by the time the capacitor needs to charge up from the reset voltage to the threshold.

Action potentials are reduced to 'events' that happen at precise moments, since their shape have always roughly the same form, thus cannot be used to transmit information.

Hodgkin-Huxley Model

The Hodgkin-Huxley (HH) model provides the foundation for modern computational neuroscience. In 1952 Alan Hodgkin and Andrew Huxley discovered the process of

the excitability of nerve fibers, through voltage-clamp circuit to enable quantitative measurement of ionic currents from a homogeneous nonmyelinated squid axon.

If the system is in its resting state and an additional electrode current pulse is applied, an action potential will be generated, as described in previous sections, and the whole process can be described with the HH equations. The equations [26] describe quantitatively the voltage current relations of a piece of membrane that includes sodium, potassium and leakage currents, in the time dimension.

The ionic current is split into components carried by sodium ions (I_{Na}), potassium ions (I_{K}) and leakage ions (I_{leak}) and can be obtained from the relations:

$$I_{\mathrm{Na}} = g_{\mathrm{Na}}(V - V_{\mathrm{Na}}) \tag{3.10}$$

$$I_{\mathrm{K}} = g_K(V - V_{\mathrm{K}}) \tag{3.11}$$

$$I_{\mathrm{leak}} = g_{\mathrm{leak}}(V - V_{\mathrm{leak}}) \tag{3.12}$$

where $V_{\mathrm{Na}}, V_{\mathrm{K}}, V_{\mathrm{leak}}$ are measured as displacements from the resting potential.

The HH equations are a set of four differential equations, represented by an electrical circuit as in Figure 3.2 and have the following form:

$$\frac{dV}{dt} = \left[- g_{\mathrm{Na}} m^3 h(V - V_{\mathrm{Na}}) - g_K n^4 (V - V_{\mathrm{K}}) - g_{\mathrm{leak}}(V - V_{\mathrm{leak}}) + I_{\mathrm{stimulus}} \right] / C_{\mathrm{m}} \tag{3.13}$$

$$\frac{dm}{dt} = \left[- (\alpha_m + \beta_m) m + \alpha_m) \right] k \tag{3.14}$$

$$\frac{dh}{dt} = \left[- (\alpha_h + \beta_h) h + \alpha_h) \right] k \tag{3.15}$$

$$\frac{dn}{dt} = \left[- (\alpha_n + \beta_n) n + \alpha_n) \right] k \tag{3.16}$$

$$k = 3^{0.1T - 0.63} \tag{3.17}$$

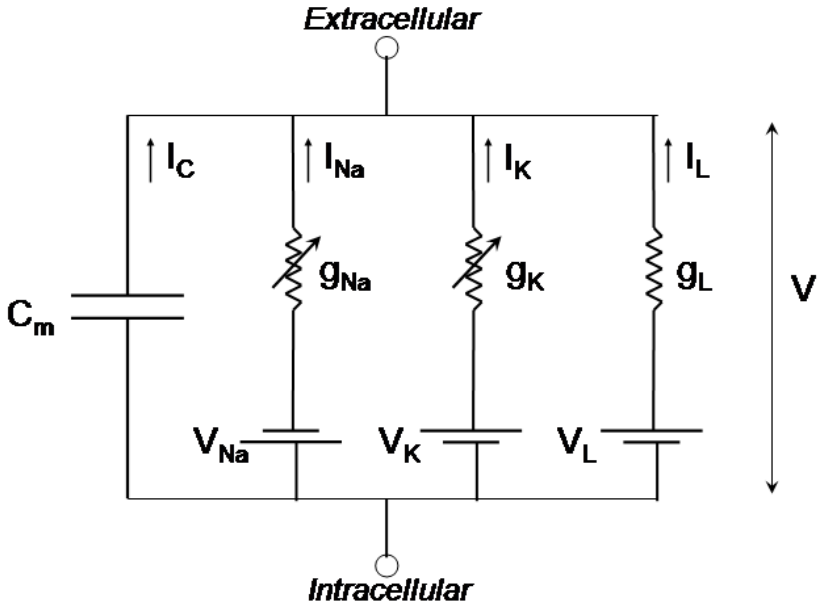

Figure 3.2: Electrical circuit representing the cell membrane according to the HH model, using the sodium, potassium and leakage currents.

V is the reduced membrane voltage, g_{Na}, g_K, g_{leak} are the maximum conductances of the channels per cm^2 that express the ionic permeability of the membrane.

The probabilities that reduce the maximum conductances of sodium and potassium according to experimental gating data are represented by the m, h, n respectively. More specifically, m is the probability for open activation gates, where 3 independent subunits are necessary for Na^+ channel to be activated (Figure 3.3), and h for open inactivation gates of the sodium channel [34]. The potassium channel can either be open or closed, therefore it has only one gating variable n, which is the probability of the channel being open (Figure 3.4). The power 4 indicates that 4 independent subunits are necessary for the K^+ channel to open.

The α and β variables are voltage-dependent transfer rate constants that do not vary with time and are fitted from experimental data to quantify the ion channel kinetics [26].

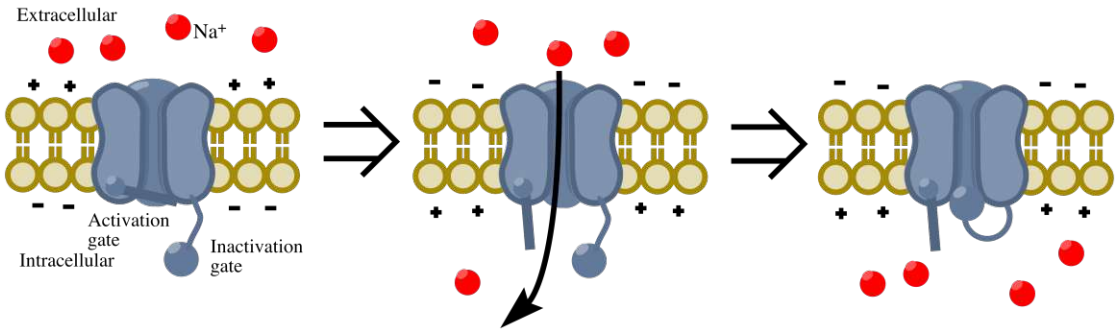

Figure 3.3: Voltage-gated sodium channel function: the activation gate is closed at rest, during the rising phase, both gates are open; during the last phase, the inactivation gate closes, whereas the activation gate remains open [56].

Based on experimental data:

$$\alpha_m = \frac{2.5 - 0.1V}{e^{2.5-0.1V} - 1} \tag{3.18}$$

$$\beta_m = 4e^{\frac{-V}{18}} \tag{3.19}$$

$$\alpha_h = 0.07e^{\frac{-V}{20}} \tag{3.20}$$

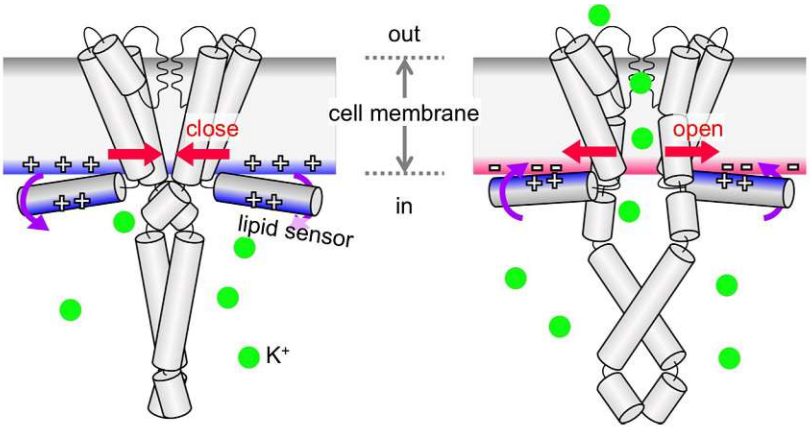

Figure 3.4: Voltage-gated potassium channel opens with a delay, at the peak potential. During and rest and in the beginning of the spike, the channel remains closed [29].

$$\beta_h = \frac{1}{e^{3-0.1V}+1} \tag{3.21}$$

$$\alpha_n = \frac{0.1-0.01V}{(e^{1-0.1V}-1)} \tag{3.22}$$

$$\beta_n = 0.125e^{\frac{-V}{80}} \tag{3.23}$$

In a more compact form where $x = m, h, n$, equations 3.14, 3.15, 3.16 can be written as:

$$\frac{dx}{dt} = \big[-(\alpha_x+\beta_x)x+\alpha_x)\big]k \tag{3.24}$$

The solution of 3.24 is:

$$x = x_0 + (x_\infty - x_0)(1-e^{-\frac{t}{\tau_x}}) \tag{3.25}$$

and satisfies the boundary condition that at $t = 0$ (before a voltage step is applied), $x = x_0$, given by:

$$x_0 = \frac{\alpha_{x_0}}{\alpha_{x_0}+\beta_{x_0}} \tag{3.26}$$

The time constant at rest is:

$$\tau_{x_0} = \frac{1}{\alpha_{x_0} + \beta_{x_0}} \tag{3.27}$$

Upon voltage change, α_{x0} and β_{x0} change instantly and we have:

$$x_\infty = \frac{\alpha_x}{\alpha_x + \beta_x} \tag{3.28}$$

$$\tau_x = \frac{1}{\alpha_x + \beta_x} \frac{1}{k} \tag{3.29}$$

where x_∞ is the steady-state value and τ_x is the time constant of the membrane for the different gating variables. The time constant is the time that the potential needs to fall from the resting state to the 63% of its value during subthreshold excitation. Regarding the gating variables, as explained above, upon change in membrane voltage there is a new equilibrium for the ion channel probability to be open/closed (or inactivated depending on the channel's states). A small time constant means that the new equilibrium is reached very quickly. Divided by the temperature factor k, τ_x becomes smaller, accelerating the gating process, for simulation temperatures T higher than the original experimental temperature of 6.3 °C.

As an example, at the resting state $t = 0$ $V(0) = 0$. For the gating variable m and from the equations 3.18 and 3.19, we get:

$$\alpha_{m_0} = \frac{2.5}{e^{2.5} - 1} = 0.224 \qquad \beta_{m_0} = 4 \tag{3.30}$$

Now 3.26 and 3.27 become:

$$m_0 = \frac{0.224}{0.224 + 4} = 0.05 \tag{3.31}$$

$$\tau_{m_0} = \frac{1}{0.224 + 4} = 0.24 \text{ ms} \tag{3.32}$$

Similarly, $h_0 = 0.6$ and $n_0 = 0.32$. Figure 3.5 shows the values of m_0, h_0, n_0 and their time constants for a specific voltage. The starting values of the gating variables when the cell is at rest can be seen in the bottom Figure 3.6, before the onset of the action potential.

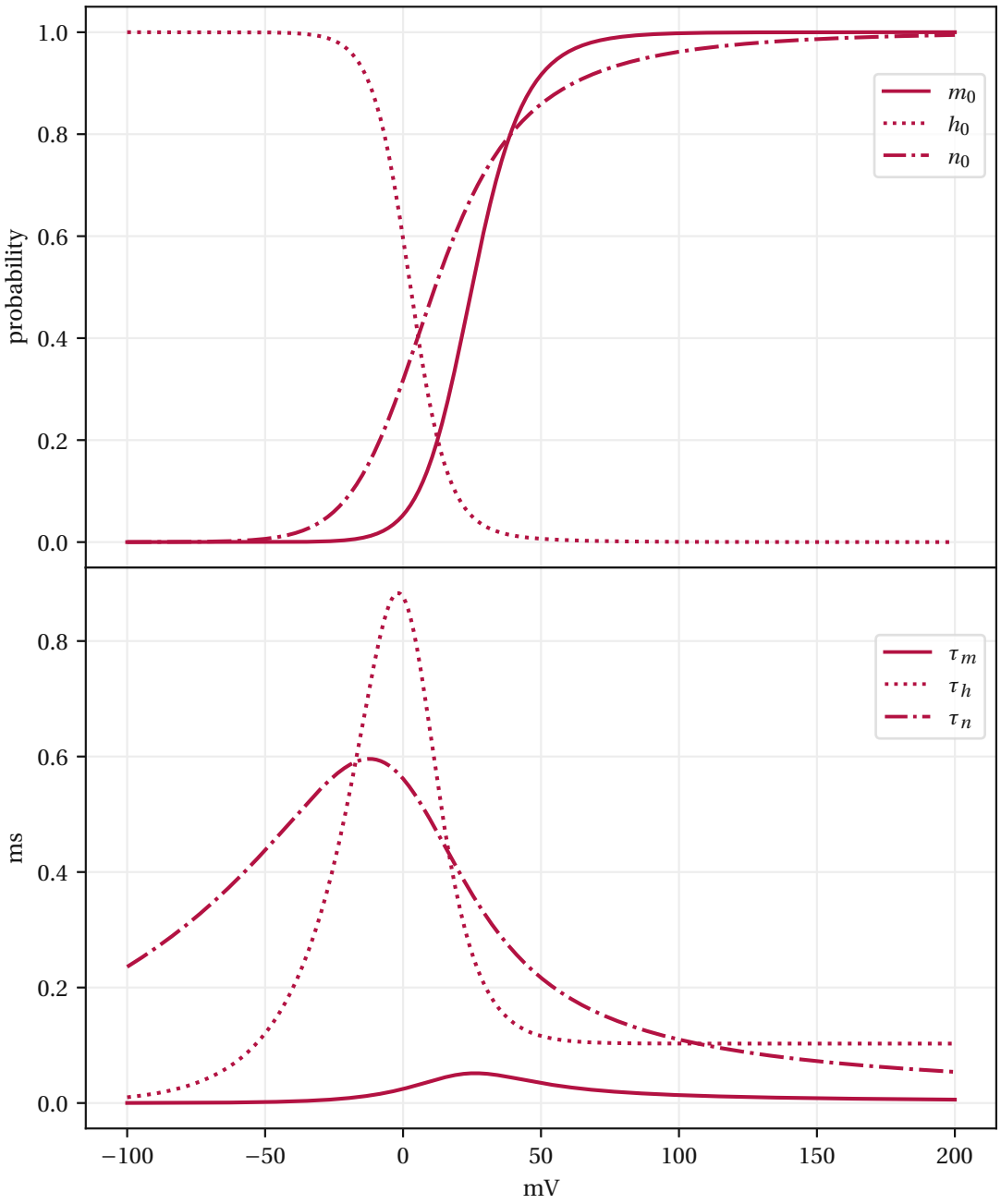

Figure 3.5: Top: Equilibrium of the different gating variables of the Hodgkin-Huxley model as functions of voltage. Bottom: The voltage dependent time constants for the activation variables m, n and inactivation variable h. Simulation temperature set to 27 °C.

The influence of temperature

When the equations 3.14, 3.15, 3.16 that describe the gating variables are multiplied by the temperature coefficient k (Equation 3.17), they influence the activation. For higher temperatures the action potential starts earlier, whereas a slower reaction is observed for decreased temperatures. High temperatures cause a shortening of the action potential duration, as well as reduction of the maximum amplitude, as can be seen in Figure 3.6.

Using the HH parameters, an action potential can no longer propagate for temperatures higher than 31 °C because of the reduced amplitude, a phenomenon known as 'heat block'.

3.2.2 HH type models

Other models of the HH type include the Frankenhaeuser and Huxley model that developed for the myelinated frog axon node, adding a nonspecific current I_p [16], and the CRRSS model on myelinated rabbit nerve node, using only calcium channel and leakage [8]. The Schwarz and Eikhof model was based on rat nodes [51], whereas the SRB (Schwarz, Reid and Bostock) model recorded in single human myelinated nerve fibres at room temperature [52].

3.3 Compartment Modeling

In silico modeling constitutes the logical extension of controlled in vitro experimentation, combining the advantages of both in vivo and in vitro experimentation [10]. There is no ethical consideration, and on the other hand having the absolute control, in silico models allow the researcher to include a virtually unlimited array of parameters, in order to create computational models that can simulate, test and predict.

However, the modeling of the real structure of a neuron is computationally expensive, therefore simplified models are created. The aim is the reduction of the complexity to the most fundamental mechanisms, yet finding and using the right parameters that achieve the simulation of the desired behavior.

The neuron is segmented into compartments with different electrical properties, as seen in the Figure 3.7, each represented by an electrical circuit with specific geom-

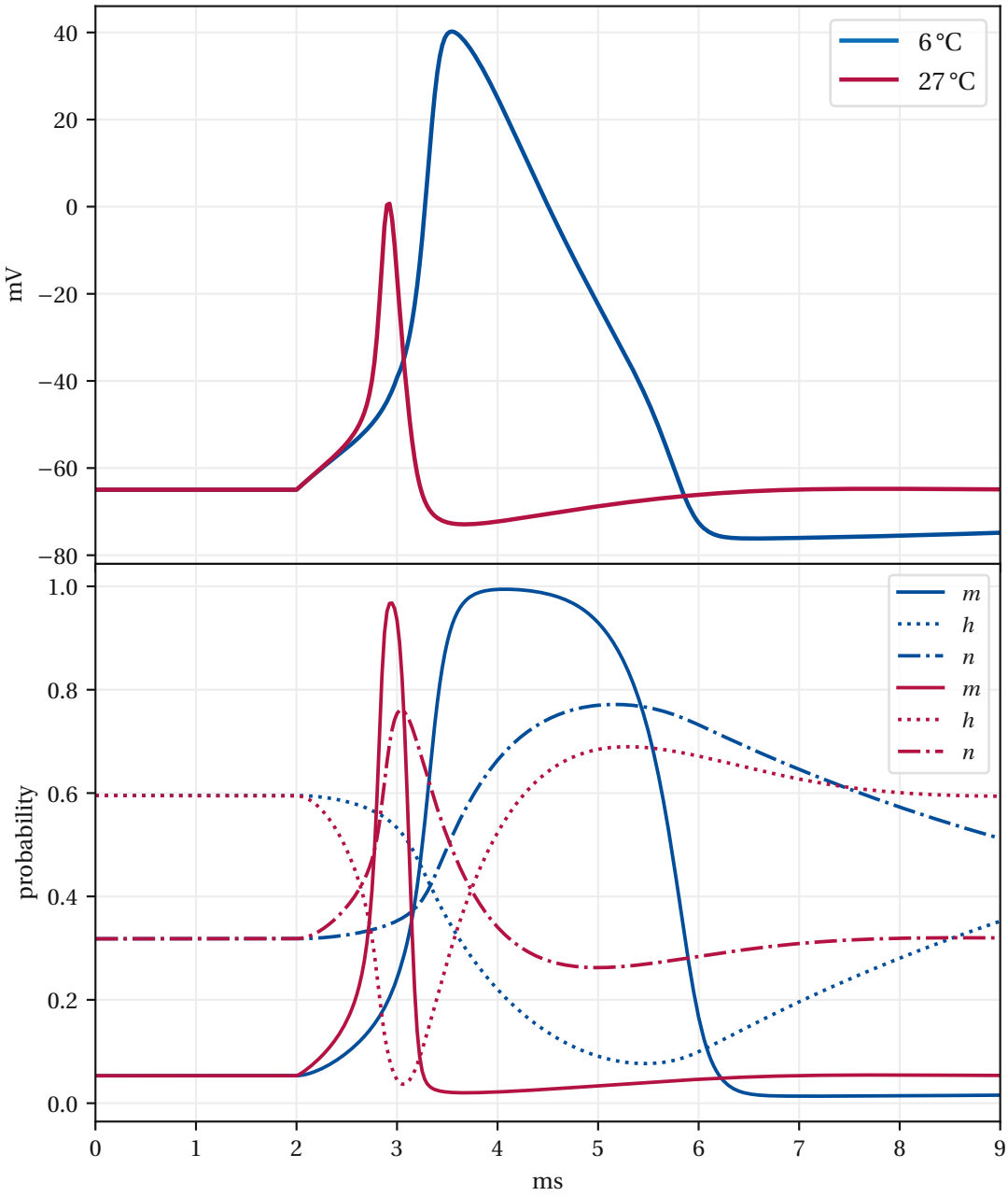

Figure 3.6: Influence of temperature in action potential: when the simulation temperature is increased from 6 °C (blue) to 27 °C (red), the activation starts earlier and the amplitude of the action potential becomes smaller. Figure on the bottom shows the behavior of the gating variables over time for the different temperatures. Probability changes last more at 6 °C.

etry and biophysical properties. Within the compartment the membrane behaves similarly, and each compartment represents a space clamp experiment, as explained in section 2.2.3.

The membrane potential is a function of distance, in contrary to the space clamp experiment, where no current flows along the fiber, meaning that there is no propagating action potential. A simultaneous spike is produced at all parts of the membrane, which is modeled as a single compartment.

The compartments are cylinders or spheres and are mathematically described by ordinary differential equations, and used to mimic and reproduce the the electrical behavior of the cell. The cylinders are connected to each other, with each treated as isopotential element (Figure 3.7). The theoretical foundation of compartment modeling is the previously described cable theory.

A simplification may be the reduction of a dendritic tree to a dendrite with just one or a few branches, or the representation of the whole cell as one, single compartment, while maintaining the dynamics of the individual conductances.

Each of these compartments is defined as the point in the middle of the geometry.

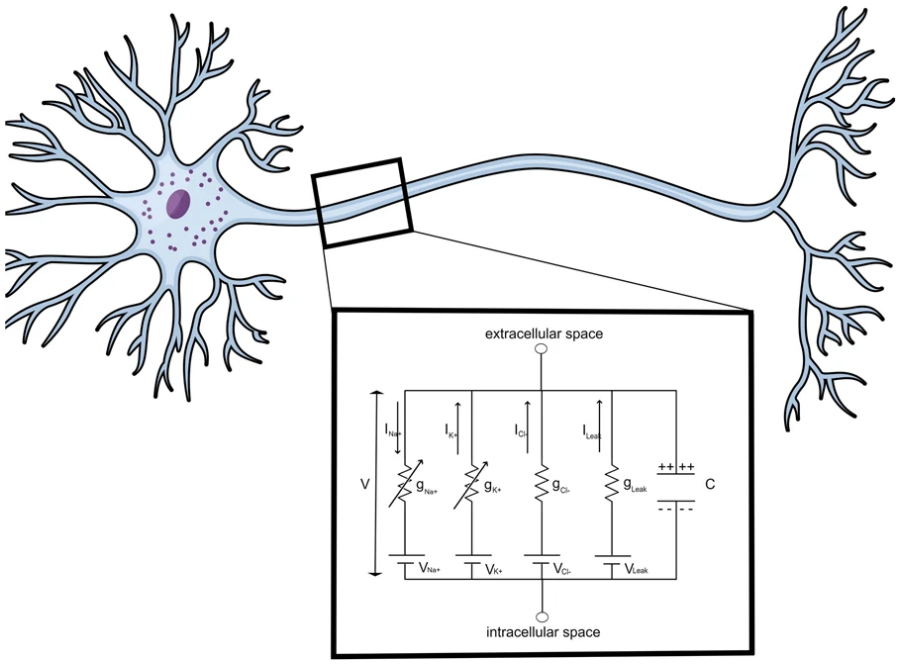

Figure 3.7: The real morphology is represented by a different number of discrete structures, based on the level of complexity and accuracy the modeler needs. The cell is an equivalent electrical network and each compartment has its own biophysics [28].

As an extension of Equation 3.8, according to Kirchhoff's law, the current in the n^{th} compartment consists of the capacitive current, the ionic current across the membrane and ohmic currents to the left and right neighbors:

$$C_{m,n}\frac{d(V_{i,n}-V_{e,n})}{dt}+I_{ion,n}+\frac{V_{i,n}-V_{i,n-1}}{R_n/2+R_{n-1}/2}+\frac{V_{i,n}-V_{i,n+1}}{R_n/2+R_{n+1}/2}=0 \tag{3.33}$$

V_i represents the intracellular voltage, R is the axial resistance and C_m is the membrane capacity.

By using the reduced voltage $V = V_i - V_e - V_{rest}$, we can compute the time courses of V_n for every compartment [47]:

$$\begin{aligned}\frac{dV_n}{dt}=\frac{1}{C_{m,n}}\Big[-I_{ion,n}+\frac{V_{n-1}-V_n}{R_{n-1}/2+R_n/2}+\frac{V_{n+1}-V_n}{R_{n+1}/2+R_n/2}+\ldots+\\ \frac{V_{e,n-1}-V_{e,n}}{R_{n-1}/2+R_n/2}+\frac{V_{e,n+1}-V_{e,n}}{R_{n+1}/2+R_n/2}+\ldots\Big]\end{aligned} \tag{3.34}$$

The dots are used in cases of more than one neighboring compartments, such as at branched regions.

3.4 Electrical Stimulation

If a stimulus current $I_{stimulus}$ is injected and if the fiber is immersed in a large volume of extracellular fluid, which means that the extracellular resistance is neglected [48], we can set $V_e = 0$ for all compartments (as long no extracellular stimulation is applied), and hence $V = V_i$ - V_{rest}. Equation 3.34 becomes:

$$\frac{dV_n}{dt}=\frac{1}{C_{m,n}}\Big[-I_{ion,n}+\frac{V_{n-1}-V_n}{R_{n-1}/2+R_n/2}+\frac{V_{n+1}-V_n}{R_{n+1}/2+R_n/2}+\ldots+I_{stimulus}\Big] \tag{3.35}$$

The membrane capacitance of each of the segment C_m, is the product of the specific membrane capacitance c_m and the segment's surface area, A:

$$C_m = c_m A \tag{3.36}$$

The half intracellular resistance between the center and the border of the compartment is:

$$\frac{R}{2} = \frac{2\rho_i l}{d^2\pi} \tag{3.37}$$

where l is the length, d is the diameter and ρ_i the intracellular resistivity of each compartment.

I_{ion} will be the product of the current density i and the surface area of the compartment:

$$I_{ion} = i_{ion} A \tag{3.38}$$

3.4.1 Influence of extracellular potential

In cases of extracellular stimulation, or transcranial magnetic stimulation, we also need to take into account the influence of the extracellular potential.

Assuming that the monopolar electrode is an ideal point source in an infinite homogeneous extracellular medium, placed at a point in a distance r from the stimulus location, the extracellular membrane voltage with an extracellular resistivity ρ_e is:

$$V_e = \frac{\rho_e I_{electrode}}{4\pi r} \tag{3.39}$$

where $I_{electrode}$ is the current of the electrode.

If now a uniform electric field (E-field) is used for the stimulation, instead of a current, the extracellular potential is given by [1]:

$$V_e = -|E| \cdot \big(x\sin(\theta)\cos(\phi) + y\sin(\theta)\sin(\phi) + z\cos(\theta)\big) \tag{3.40}$$

where E represents the amplitude of the electric field in $\mathrm{V\,m^{-1}}$, and (x, y, z) are the coordinates of each compartment (in NEURON this is the middle of the segment). The E-field is a vector that only depends on the amplitude (strength of the field), as well as the polar angle θ and azimuthal angle ϕ, that define the direction of the field. The center of the soma is the origin of the spherical coordinates.

The electric field is the difference in voltage between two locations in the brain. In general, two parallel plates form an electric field separated by a distance and attached to a battery with a voltage, produce a uniform electric field. At any point between the plates the strength of the electric field acting on a charge is constant. The

electric field lines are equally spaced, straight and parallel, and point in the direction of force that a positive test charge would experience. The lines can never cross, they are perpendicular to the surface they come from, and move away from the positive towards the negative plate (direction of positive test charge) as Figure 3.8 shows.

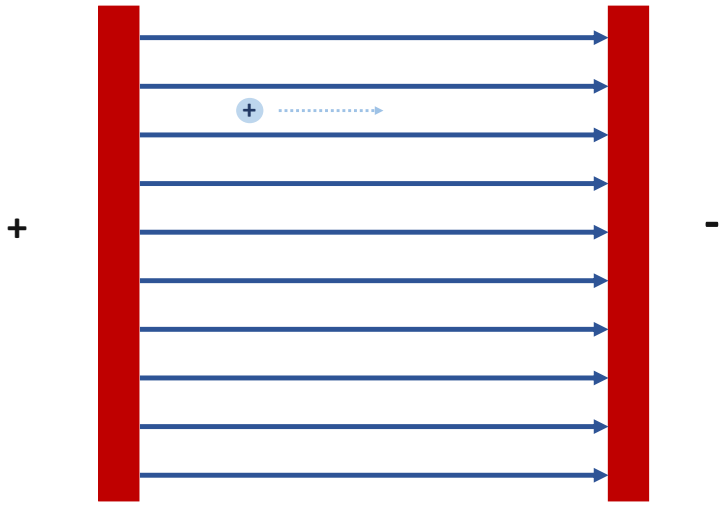

Figure 3.8: The electric field between oppositely charged plates is uniform, except at the edges. A positive charge in the uniform E-field is repelled by the positive plate and moves towards the negative plate.

It can be defined as:

$$E = \frac{F}{q} \tag{3.41}$$

where E is the electric field, F is the electric force in Newton (N) and q is the charge in Coulomb (C). In the uniform case, it can be also thought as how big a voltage is applied to the plates and how far apart they are:

$$E = \frac{V}{d} \tag{3.42}$$

where V is the voltage across the plates in Volts (V) and d is the distance of the two separated plates.

Activating Function

The direct stimulating influence of the extracellular potential on the nth compartment is called the activating function f_n [45]:

$$f_n = \frac{1}{C_{m,n}}\left[\frac{V_{e,n-1} - V_{e,n}}{R_{n-1}/2 + R_n/2} + \frac{V_{e,n+1} - V_{e,n}}{R_{n+1}/2 + R_n/2} + ...\right] \tag{3.43}$$

The first and last compartment only have one neighboring segment, so the equation 3.43 has a reduced form. In the bifurcations of branched regions some extra terms need to be added, as indicated by the dots.

The activating function is the second derivative of the extracellular potential along the unmyelinated fiber, and the second difference quotient of the extracellular potential for a myelinated axon. It represents the direct influence of the electric field in every compartment n of the model. That is the rate of membrane voltage change activated by the extracellular field, when the neuron is at rest before stimulation, or the slope of membrane voltage at the beginning of the stimulus.

In this form, the activating function is the velocity of the voltage change in each compartment due to the extracellular field.

Using the reduced membrane voltage, in the beginning of the stimulation the membrane potential will be zero. Consequently, the areas where the activation function f is positive, will be the region of the fiber that is extracellularly stimulated. The origin of an artificially generated action potential is expected in the region where f has the highest value (Figure 3.9).

When a cathodic current is applied, the depolarized area will be under the electrode, whereas the regions on the sides will be hyperpolarized; anodic currents result in hyperpolarized region under the electrode, and depolarized regions on the two sides, as shown in Figure 3.10.

Contrary to intracellular stimulation, in most cases of extracellular stimulation, better results are achieved with cathodic pulses [45], [49], [62].

In cathodic stimulation, negatively charged anions flow from the cathode, into the tissue, and back to the anode. As the electrical current flows from cathode to anode, negative charges (anions) tend to accumulate on the outer surface of the nerve membrane as they will be repelled by the negatively charged cathode, making the outside of the membrane more negative. Consequently, the inside of the membrane

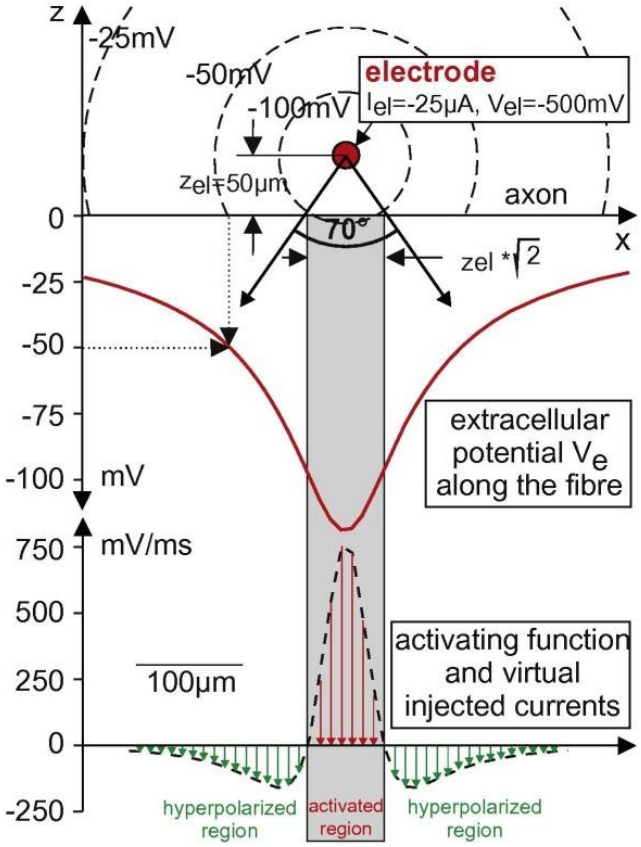

Figure 3.9: Extracellular stimulation with cathodic current and a point source placed 50 µm above the fiber (upper); computation of extracellular potential using Equation 3.39 (middle); the activating function is positive and has its peak value in the activated region, that is where the cell is depolarized (lower) - in the outside regions the stimulation results in hyperpolarization. [50].

becomes more positive due to accumulation of positive ions on the inside, which results in depolarization, and if it is sufficient, it will result in an action potential.

The action potential generated at the depolarized area can propagate through the hyperpolarized site, if the hyperpolarization is not too large [44].

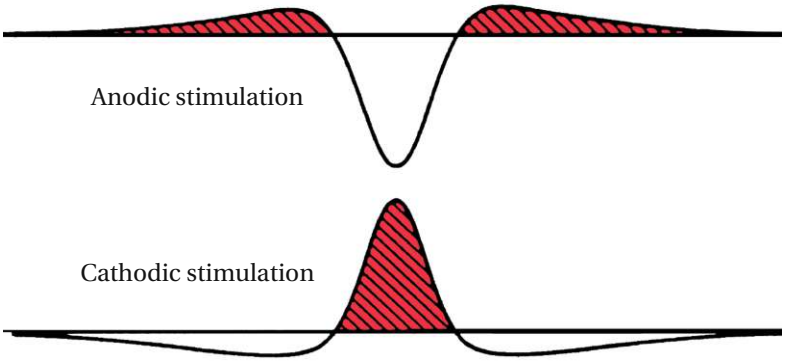

Figure 3.10: The activation function for anodic and cathodic current pulses (Figure modified from [46]).

Chapter 4

Modeling a Martinotti Cell

This thesis presents the results of the simulations of a Martinotti cell modeled as a single compartment cell, and using a more complex geometry, as a linear and 3D multi compartment neuron.

The simulations were implemented in NEURON [6] and Python [61]. The intracellular stimulations were performed in the Python interface of NEURON, whereas for the extracellular stimulations and TMS with a uniform electric field Python was used exclusively.

4.1 Implementation Details

4.1.1 NEURON

NEURON is a simulation environment for modeling neurons and networks of neurons, developed by J. Moore, M. Hines and T. Carnevale. It gives the possibility of being incorporated and work within the Python context alone, or in combination with NEURON's traditional Hoc, an interpreted language with C-like syntax [24]. The interface was designed as an intuitive environment, hiding the details of the numerical methods used in the simulation.

Each section in NEURON is a continuous unbranched cable and can be connected with other sections to form branched trees. The sections can further be divided into segments of equal length, whose number define the number of internal points at which the discretized form of the cable equation is integrated [25].

The section is described in terms of normalized distance, with 0 denoting the start and 1 the end of the section and can be used to specify the location of the electrodes.

For each section the geometry (diameter, length, number of segments), the biophysical properties (axial resistivity, capacitance, conductances), as well as the connectivity can easily be defined.

The 3D geometry specifies the section's shape, orientation, and location in three dimensions. The first point of each section is the same as the last point of the previous one (if there is a parent section).

4.1.2 Single Compartment Model

The cell was modeled as a spherical soma with a diameter of 67 µm, based on the properties of [32], with only one compartment. The intracellular resistivity (axial/cytoplasmatic resistivity in NEURON) is set to $R_a = 100\,\Omega\,\mathrm{cm}$ and the specific membrane capacitance is set to $c_m = 1\,\mu\mathrm{F\,cm^{-2}}$.

The model is loaded with the passive mechanism 'pas' of NEURON, as well as other mechanisms, representing the active membrane. These biophysics are based on the scientific articles of [32, 40], where a single compartment HH type neuron model was developed, described by the membrane equation:

$$C_m \frac{dV}{dt} = -g_{leak}(V - E_{leak}) - I_{Na} - I_K - I_M - I_T \tag{4.1}$$

where the first current term represents the leakage current: g_{leak} is the leak membrane conductance, E_{leak} is the resting membrane reversal potential. The kinetics deployed are based on the `MOD` files of the [40] as presented in the Model DB [36] and are presented below.

The voltage dependent sodium current is modeled using the equations:

$$
\begin{aligned}
i_{\mathrm{Na}} &= g_{\mathrm{Na}} m^3 h (V - E_{\mathrm{Na}}) \\
\frac{dm}{dt} &= \left[\alpha_m(V)(1-m) - \beta_m(V) m\right] k \\
\frac{dh}{dt} &= \left[\alpha_h(V)(1-h) - \beta_h(V) h\right] k \\
\alpha_m &= \frac{-0.32(V - V_{\mathrm{T}} - 13)}{\exp\left[\frac{-(V - V_{\mathrm{T}} - 13)}{4}\right] - 1} \\
\beta_m &= \frac{0.28(V - V_{\mathrm{T}} - 40)}{\exp\left[\frac{V - V_{\mathrm{T}} - 40)}{5}\right] - 1} \\
\alpha_h &= 0.128 \exp\left[\frac{-(V - V_{\mathrm{T}} - 17)}{18}\right] \\
\beta_h &= \frac{4}{\exp\left[\frac{-(V - V_{\mathrm{T}} - 40)}{5}\right] + 1}
\end{aligned}
\tag{4.2}
$$

The kinetics of the voltage dependent potassium current (delayed rectifier) are:

$$
\begin{aligned}
i_{\mathrm{K}} &= g_{\mathrm{K}} n^4 (V - E_{\mathrm{K}}) \\
\frac{dn}{dt} &= \left[\alpha_n(V)(1-n) - \beta_n(V) n\right] k \\
\alpha_n &= \frac{-0.032(V - V_{\mathrm{T}} - 15)}{\exp\left[\frac{-(V - V_{\mathrm{T}} - 15)}{5}\right] - 1} \\
\beta_n &= 0.5 \exp\left[\frac{-(V - V_{\mathrm{T}} - 10)}{40}\right]
\end{aligned}
\tag{4.3}
$$

The variable V_{T} is used for adjusting the spike threshold and is set to -63 mV.

The voltage dependent M current is a slow non-inactivating potassium current, responsible for spike-frequency adaptation, described by [65] with maximum conductance g_{M} and defined as:

$$
\begin{aligned}
i_{\mathrm{M}} &= g_{\mathrm{M}} p (V - E_{\mathrm{K}}) \\
\frac{dp}{dt} &= \frac{p_\infty(V) - p}{\tau_p(V)} \\
p_\infty(V) &= \frac{1}{\exp\left[\frac{-(V+35)}{10}\right] + 1} \\
\tau_p(V) &= \frac{\tau_{\max}}{3.3 \exp\left[\frac{V+35}{20}\right] + \exp\left[\frac{-(V+35)}{20}\right]} \frac{1}{k}
\end{aligned}
\tag{4.4}
$$

where $\tau_{\max} = 1000$ ms.

The kinetics of the low threshold calcium current, initially designed for thalamic neurons with maximum conductance the g_T are presented in [40]:

$$
\begin{aligned}
i_T &= g_T s_\infty^2 u(V - E_{Ca}) \\
\frac{u}{dt} &= \frac{u_\infty(V) - u}{\tau_u(V)} \\
s_\infty(V) &= \frac{1}{\exp\left[\frac{-(V+V_x+57)}{6.2}\right] + 1} \\
u_\infty(V) &= \frac{1}{\exp\left[\frac{V+V_x+81}{4}\right] + 1} \\
\tau_u(V) &= \frac{30.8 + 211.4 + \exp\left[\frac{V+V_x+113.2}{5}\right]}{1 + \exp\left[\frac{V+V_x+84)}{3.2}\right]} \frac{1}{k}
\end{aligned}
\tag{4.5}
$$

where V_x is a uniformal shift of the voltage dependence and is set to 2 mV.

All channels are also influenced by the temperature coefficient k as described in 3.17 and 3.2.1, which is given by:

$$
\begin{aligned}
k &= 3^{\frac{x-36}{10}} \\
k &= 2.3^{\frac{x-36}{10}} \\
k &= 3^{\frac{x-24}{10}}
\end{aligned}
\tag{4.6}
$$

for the sodium & potassium channels, the M current, and the T current respectively. The simulation temperature is represented by x.

The parameters used for the single compartment model are presented in Table 4.1. The conductances are in $S\,cm^{-2}$ and the reversal potentials in mV.

This model was tested with and without the T current in order to examine its effect on the intracellular simulation for a duration of 1 ms.

4.2 Multicompartment Model

The next step is to build a simple, but more complex than the previously presented model, by using more than one sections segmented into compartments.

This first approach is a linear model containing a non-branching dendrite, a spherical soma with only one compartment and a stick myelinated axon.

SINGLE COMPARTMENT MODEL

	soma
g_{leak}	0.00015
E_{leak}	-70
g_K	0.01
E_K	-100
g_{Na}	0.05
E_{Na}	50
g_M	0.0001
g_T	0.0004
E_{Ca}	120
c_m	1
R_a	100

Table 4.1: Parameters of the single compartment model.

The model that resembles the most a real morphology is the 3D model, which has a branching dendrite and a long non-myelinated branching axon.

4.2.1 Linear Model

Morphology

The linear model is mostly based on the model of neuron 1 presented in the paper [50] and consists of a non-tapering dendrite of diameter 1 µm, spherical soma of reduced diameter 30 µm, axon hillock with diameter of 3.1 µm, axon initial segments (ais) with a slightly higher diameter of 1.22 µm, than the naked axon of 1 µm. The myelinated axon has a total length of 500 µm and consists of alternating nodes of Ranvier and internodes, five each. The internodes have the diameter of the naked axon, whereas the nodes have a reduced diameter of 0.75 µm.

The end of the axon comprises an unmyelinated terminal as can be seen in Figure 4.1. Details about the geometry and segmentation of the model can be found in Table 4.2.

The neuron lies on the x axis, with the middle of the soma being placed at the origin (0, 0). Every section is connected at the end 1 of the parent section.

The diameter of the soma was reduced more than half, so that the dendritic spikes

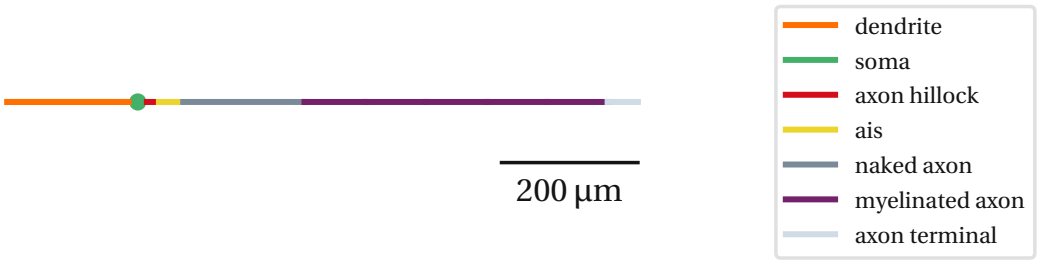

Figure 4.1: Morphology of the linear model lying on the x axis.

LINEAR MODEL

	length	diameter	# of segments
dendrite	200	1	20
soma	30	30	1
axon hillock	10	3.1	2
ais	50	1.22	2
naked axon	200	1	15
internode	99	1	1
node of Ranvier	1	0.75	1
terminal	50	1	8

Table 4.2: Geometry of the linear model: lengths and diameters in µm.

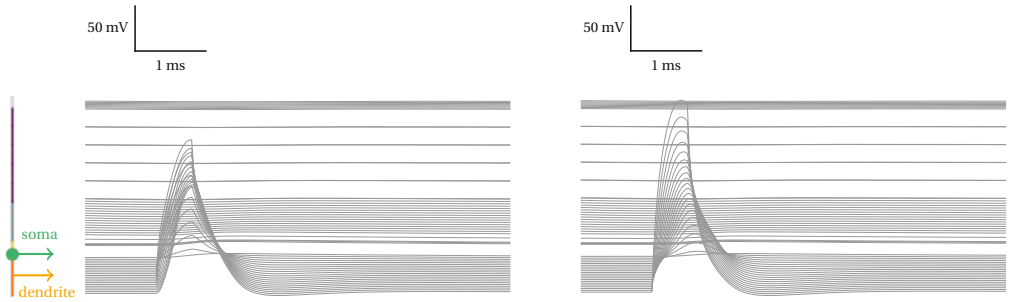

(a) Stimulation in the middle of the dendrite.

(b) Stimulation at the dendritic end.

Figure 4.2: Intracellular stimulations in the dendrite of the linear model with suprathreshold pulses of 2 nA for 0.5 ms result in non-propagating action potentials due to the large spherical soma (diameter = 67 µm). The lines on the bottom of the figure represent the dendritic membrane potential, and those on the top show the axonal voltage. The gaps between the lines denote the distance of two consecutive compartments.

can propagate to the soma and down the axon. As we know from the bibliography, Martinotti cells have a small cell body [63]. For the initial diameter of 67 µm and during dendritic stimulation in the middle or at the end of the neuronal process no spike was initiated. The large capacitance of the soma consumes by its loading the intracellular current coming from the dendrite to such an extend, that is not able to exceed the threshold voltage, as Figure 4.2 shows.

From additional tests, we can see that by increasing the proximal part of the dendritic diameter, a larger spherical soma is able to be excited (Figure 4.3). A spike could be generated with the use of a tapering dendrite, with a diameter of 1 µm in the proximal part, and a larger of 2.5 µm in the distal part. The maximum soma diameter was found to be 50 µm.

Biophysics

Regarding the biophysics, the neuron has been modeled using the kinetics of a Martinotti cell for the dendrite and soma processes, as previously described in the single compartment model. More specifically, the soma contains all but the calcium channel, with the same densities as before, whereas for the dendrite, the T calcium channel has been added to the sodium and potassium channels. As stated in [20], low voltage activated T type calcium channels are expressed at high densities on den-

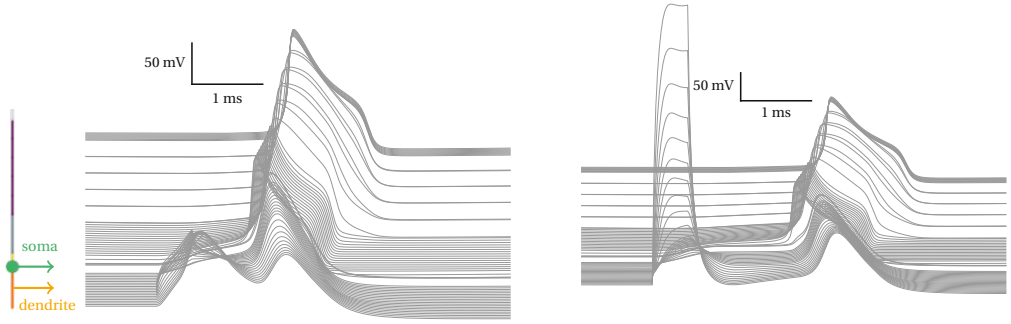

(a) Stimulation in the middle of the dendrite.

(b) Stimulation at the dendritic end results in an extremely high voltage which decays over time and propagates down the axon.

Figure 4.3: Dendritic stimulations inside the cell of the linear model for 0.5 ms. Threshold pulses are 8 nA and 2.5 nA respectively. Here we are using a large, but smaller (diameter = 50 µm) than the initial soma (diameter = 67 µm) and a tapering dendrite. The lines on the bottom of the figure represent the dendritic membrane potential, and those on the top correspond to the voltage in the axon. The gaps between the lines denote the distance of two consecutive compartments.

drites of low threshold spiking interneurons.

The densities of the sodium and potassium channels are now decreased, using the factor 0.7 of the soma's densities.

The axonal part has been modeled as an L5 pyramidal cell, using the ion channels of the axon of neuron 1 of [50]. The kinetics of the ion channels are modified and obtained from the published article of [27] and the Model DB [36].

The sodium channels deployed are the low threshold $g_{\mathrm{Na_v}1.6}$ and high threshold $g_{\mathrm{Na_v}1.2}$ with the highest value of the maximum conductances being $0.32\,\mathrm{S\,cm^{-2}}$ in the axon initial segments and in the axon hillock respectively.

The maximum conductance of the potassium current is in the unmyelinated axon with a value $0.15\,\mathrm{S\,cm^{-2}}$.

The myelin sheath is rich in lipids and acts as an insulator, meaning that it has a high transverse resistance and low capacitance. Therefore it has been simulated using 17 layers, resulting in a reduced membrane capacitance of $0.0588\,\mu\mathrm{F\,cm^{-2}}$, compared to the $1\,\mu\mathrm{F\,cm^{-2}}$ of the rest of the cell membrane.

As stated in [5] $\mathrm{Na_v}1.6$ are highly concentrated at the nodes of Ranvier of neurons in the central nervous system, thus this sodium channel is only present in the myelin gap, whereas the internodes contain $\mathrm{Na_v}1.2$ (this is the only active mechanism of the internodes) with the density of $0.02\,\mathrm{S\,cm^{-2}}$.

LINEAR MODEL

	dendrite	soma
g_{leak}	0.000105	0.00015
E_{leak}	-70	-70
g_K	0.007	0.01
E_K	-100	-100
g_{Na}	0.035	0.05
E_{Na}	50	50
g_M	0.00007	0.0001
g_T	0.0004	
E_{Ca}	120	120
c_m	1	1
R_a	100	100

Table 4.3: Channel densities of linear model in $S\,cm^{-2}$: dendrite and soma. Reversal potentials in mV, resistivity in $\Omega\,cm$, capacitance in $\mu F\,cm^{-2}$.

Background leak conductance is distributed throughout the axon with a density of $0.000\,033\,S\,cm^{-2}$, except for the myelinated axon. In the internodes this value has been decreased by dividing it by the number of the sheets. In the nodes of Ranvier this value is increased to $0.02\,S\,cm^{-2}$.

The reversal potential of the leak current in all sections is set to $-70\,mV$, and the axial resistivity $R_a = 100\,\Omega\,cm$. All values are shown in detail in Tables 4.3 and 4.4.

The equations that describe the kinetics of the ion channels expressed in the axon are presented below. Note that unlike the Equations 3.14 - 3.16, the temperature coefficient k is now multiplied by the ionic currents and not by the equation describing the rate of change of the gating variables [27, 36].

K channel:

LINEAR MODEL

	axon hillock	ais	naked axon	internodes	nodes	terminal
g_{leak}	0.000033	0.000033	0.000033	0.00000194117	0.02	0.000033
E_{leak}	-70	-70	-70	-70	-70	-70
g_K	0.1	0.1	0.15		0.02	0.02
E_K	-90	-90	-90		-90	-90
$g_{Na_v1.2}$	0.32	0.13	0	0.02	0	0
$g_{Na_v1.6}$	0	0.32	0.3		0.16	0.16
E_{Na}	60	60	60		60	60
c_m	1	1	1	0.059	1	1
R_a	100	100	100	100	100	100

Table 4.4: Channel densities of linear model in $S\,cm^{-2}$: axon. Reversal potentials in mV, resistivity in $\Omega\,cm$, capacitance in $\mu F\,cm^{-2}$.

$$
\begin{aligned}
I_K &= k g_K n (V - E_K) \\
\alpha_n &= \frac{0.02(V-25)}{1-\exp\left[\frac{-(V-25)}{9}\right]} \\
\beta_n &= \frac{-0.002(V-25)}{1-\exp\left[\frac{V-25}{9}\right]} \\
\frac{dn}{dt} &= \alpha_n(V)(1-n) - \beta_n(V) n \\
k &= 2.3^{\frac{x-23}{10}}
\end{aligned}
\tag{4.7}
$$

For the sodium channels the currents and temperature coefficients are described by:

$$
\begin{aligned}
I_{Na} &= k g_{Na} m^3 h \\
k &= 2.3^{\frac{x-23}{10}}
\end{aligned}
\tag{4.8}
$$

For the $Na_v1.2$ channel we have:

$$
\begin{aligned}
\alpha_m &= \frac{0.182(V+28)}{1-\exp\left[\frac{-(V+28)}{7}\right]} \\
\beta_m &= \frac{0.124(-V-28)}{1-\exp\left[\frac{-(-V-28)}{7}\right]} \\
\frac{dm}{dt} &= \alpha_m(V)(1-m) - \beta_m(V)m \\
\alpha_h &= \frac{0.024(V+35)}{1-\exp\left[\frac{-(V+35)}{5}\right]} \\
\beta_h &= \frac{0.0091(-V-60)}{1-\exp\left[\frac{-(-V-60)}{5}\right]} \\
\tau_h &= \frac{1}{a+b} \\
h_\infty &= \frac{1}{1+\exp\left[\frac{V+57}{6.2}\right]}
\end{aligned}
\tag{4.9}
$$

And for the $Na_v1.6$:

$$
\begin{aligned}
\alpha_m &= \frac{0.182(V+41)}{1-\exp\left[\frac{-(V+41)}{6}\right]} \\
\beta_m &= \frac{0.124(-V-41)}{1-\exp\left[\frac{-(-V-41)}{6}\right]} \\
\frac{dm}{dt} &= \alpha_m(V)(1-m) - \beta_m(V)m \\
\alpha_h &= \frac{0.024(V+41)}{1-\exp\left[\frac{-(V+41)}{5}\right]} \\
\beta_h &= \frac{0.0091(-V-73)}{1-\exp\left[\frac{-(-V-73)}{5}\right]} \\
\tau_h &= \frac{1}{a+b} \\
h_\infty &= \frac{1}{1+\exp\left[\frac{V+70}{6.2}\right]}
\end{aligned}
\tag{4.10}
$$

4.2.2 3D Model

The 3D model has a more complex geometry with branched dendrite and axon and is closer to a real morphology. Simplifications have been made by pruning the trees of the axonal process. The axon consists of the axon hillock, the unmyelinated part

and the axon terminals.

Morphology

The geometry of the soma and dendrite consists of the real coordinates of an L5 Martinotti cell found in the cerebral cortex of a mouse and is available in `neuromorpho.org` [23].

This is a centrally curated inventory of digitally reconstructed neurons. Morphological data can be used for analysis, visualization, and modeling. Each neuron in `neuromorpho.org` is represented `ASCII` files of the digital morphological reconstruction, and a set of morphometric features.

The `swc` file defines the traced coordinates in the three-dimensional space, and gives information about the radius and the structure identifier of the cell. The latter specifies the type of the section: number 1 corresponds to the soma, 2, to the axon and 3 is the dendrite. The axonal part has been discarded, and instead the axonal part of another cell has been used.

The diameter of the soma was reduced to 30 µm, from the original 60.4 µm, to achieve propagation of the action potential to the axon, as in the case of our linear model presented above. Moreover this reduced diameter value is closer to already published data. In this case the soma consists of two linear segments.

The information of the `swc` file was 'translated' with the use of Python pandas `DataFrame` as a labeled data structure. A directed graph was then created with the Python library `NetworkX`. Each 3D point represented a node which carries the sample number, and the Euclidean distance between the coordinates of two neighboring nodes defines the corresponding edge. By keeping the nodes that have exactly one predecessor and one successor, the corresponding edges formed all possible branches. These branches needed to be ordered by finding the shortest path between the two nodes that have a degree different form two. For each of the ordered branches, the structure identifier of each node was checked; if a node had a different identifier than the previous node in the list, a new section was created.

The somatodendritic part was then connected to the axon of a real 3D L5 Martinotti cell morphology of a rat's somatosensory cortex. The data were obtained from the repository of EPFL's Blue Brain Project (BBP) [35].

The BBP is a Swiss brain research Initiative aiming to establish simulation neuroscience as a complementary approach, achieved by building the world's first biologically detailed digital reconstructions and simulations of the mouse brain.

From the `asc` file and after discarding the soma and dendrite coordinates, a directed graph was again created for the axonal part this time. By adding a virtual node, the edges could represent a section.

For simplification and computational efficiency reasons, we only use some of the axonal branches of the original geometry. Five axonal branches in descending order have been used; the first is the longest branch originating from the soma, as Figure 4.4a a shows.

The axon terminals are the 0.7 % of the axon's total length, and the axon hillock is the first part of the longest branch, with a length of 7% the total's.

The simplified axon was then connected to the soma and dendrite using NEURON'S methods and the final 3D model was created. The model was projected onto the $xy-$ plane and was horizontally flipped (Figure 4.4b. As mentioned previously, the dendrites of Martinotti cells are in the lower layers of the cerebral cortex and have their axons projecting to Layer 1.

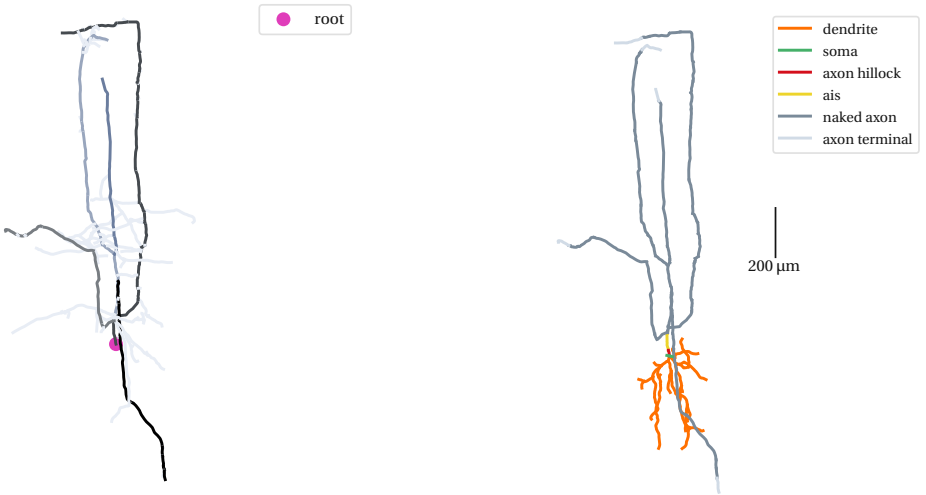

(a) Original branched axon [35] of an L5 Martinotti cell, with the 5 longest branches highlighted in darker shades of blue. Root denotes the origin of axons.

(b) Simplified morphology of the 3D model, with branched dendrite [23] and simplified bifurcated axon of (a).

Figure 4.4: Morphology of the 3D model on the $xy-$ plane.

Biophysics

The biophysics of the soma and dendrite are exactly the same as those described for the linear model. The axon is modeled again using the biophysics of a Pyramidal cell, as the axon of neuron 2 in [50]. Hence, the original parameters of [27] were used.

Potassium channel kinetics have already been described. For the sodium channels the equations are presented below:

$$\begin{aligned} I_{\mathrm{Na}} &= k g_{\mathrm{Na}} m^3 h \\ k &= 2.3^{\frac{x-23}{10}} \end{aligned} \tag{4.11}$$

For the $\mathrm{Na_v}1.2$ channel:

$$\begin{aligned} \alpha_m &= \frac{0.182(V+43)}{1-\exp\left[\frac{-(V+43)}{7}\right]} \\ \beta_m &= \frac{0.124(-V-43)}{1-\exp\left[\frac{-(-V-43)}{7}\right]} \\ \frac{dm}{dt} &= \alpha_m(V)(1-m) - \beta_m(V)m \\ \alpha_h &= a_h = \frac{0.024(V+50)}{1-\exp\left[\frac{-(V+50)}{5}\right]} \\ \beta_h &= b_h = \frac{0.0091(-V-75)}{1-\exp\left[\frac{-(-V-75)}{5}\right]} \\ \tau_h &= \frac{1}{a+b} \\ h_\infty &= \frac{1}{1+\exp\left[\frac{V+72}{6.2}\right]} \end{aligned} \tag{4.12}$$

And for the $Na_v1.6$:

$$
\begin{aligned}
\alpha_m &= \frac{0.182(V+43)}{1-exp[\frac{-(V+43)}{6}]} \\
\beta_m &= \frac{0.124(-V-43)}{1-\exp\left[\frac{-(-V-43)}{6}\right]} \\
\frac{dm}{dt} &= \alpha_m(V)(1-m)-\beta_m(V)m \\
\alpha_h &= \frac{0.024(V+50)}{1-\exp\left[\frac{-(V+50)}{5}\right]} \\
\beta_h &= \frac{0.0091(-V-75)}{1-\exp\left[\frac{-(-V-75)}{5}\right]} \\
\tau_h &= \frac{1}{a+b} \\
h_\infty &= \frac{1}{1+\exp\left[\frac{V+72}{6.2}\right]}
\end{aligned}
\tag{4.13}
$$

The details of the channel densities and reversal potentials are shown in Table 4.5.

This time, the axon's parts are the axon hillock, the axon initial segment, the unmyelinated axonal part and axon terminals. For the latter, the biophysics are those used for the nodes of Ranvier in the linear model. The maximum potassium conductance was reduced to $0.02\,\mathrm{S\,cm^{-2}}$, and the maximum sodium conductance for $Na_v1.6$ was decreased to $0.16\,\mathrm{S\,cm^{-2}}$. The maximum leakage conductance was kept the same, $3\times10^{-5}\,\mathrm{S\,cm^{-2}}$.

3D MODEL

	dendrite	soma	axon hillock	ais	unmyelinated axon	axon terminal
g_{leak}	0.000105	0.00015	0.000033	0.000033	0.000033	0.000033
E_{leak}	-70	-70	-70	-70	-70	-70
g_K	0.007	0.01				
E_K	-100	-100				
g_{Na}	0.035	0.05				
E_{Na}	50	50				
g_M	0.00007	0.0001				
g_T	0.0004					
E_{Ca}	120	120				
g_K			0.1	0.1	0.15	0.02
E_K			-90	-90	-90	-90
$g_{Na_v1.2}$			0.32	0.1	0	0
$g_{Na_v1.6}$			0	0.32	0.3	0.16
E_{Na}			60	60	60	60
c_m	1	1	1	1	1	1
R_a	100	100	100	100	100	100

Table 4.5: Channel densities of 3D model in $S cm^{-2}$, reversal potentials in mV, resistivity in Ωcm, capacitance in $\mu F cm^{-2}$.

Chapter 5

Results

5.1 Simulation Details

All presented results are simulated for 36 °C. Original soma diameter of 67 µm was used for the single compartment model simulated as a sphere (Section 4.1.2) and smaller spherical soma of 30 µm for the linear model. The 3D model consists of two linear sections of diameter 30 µm, as described in Section 4.2.2.

5.1.1 Electrical Stimulation

The linear and 3D models were stimulated intracellularly with anodic current pulses of different amplitudes in different positions, until the threshold voltage was found using the `IClamp` point process of NEURON.

For the extracellular stimulation the activating function (Equation 3.43) was used to describe the extracellular influence. The extracellular potential V_e was approximated only by an ohmic resistance, as stated in Equation 3.39. Only cathodic current square pulses were tested as they lead to more efficient stimulation results [44, 45, 49, 62].

The spherical stimulating electrode was placed 50 µm above the cell, and the ground electrode was considered relatively far away from the stimulating electrode. Moreover, the intracellular resistivity ρ_i has the same value as in the linear model 100 Ω cm and the extracellular is set to $\rho_e = 300\,\Omega\,\text{cm}$.

For the extracellular stimulation, the Python solver `odeint` was used with a time step of 0.01 ms.

The duration of the stimuli was 0.5 ms for the intra and extracellular stimulations of the multicompartment models and 1 ms for the single compartment model.

The linear model has been stimulated in and above the dendritic end and the middle of the dendrite, the soma and the axon terminal. For the 3D model additional point of interest was the turning point (kink) of the longest axonal branch. The axon stimulated in the 3D model was the longest axonal branch, similarly to the dendritic stimulation, where again the longest branch has been tested.

5.1.2 Transcranial Magnetic Stimulation

The Python solver `odeint` with the same time step of 0.01 ms was also used for the stimulation of the multicompartment models with a uniform electric field.

Similarly to extracellular stimulation, a binary search was used for determining the threshold amplitude, sufficient to elicit an action potential with rectangular pulses, with an accuracy higher than $0.5\,\mathrm{V\,m^{-1}}$ for the E-field stimulation in the linear model. For the 3D model the accuracy was $50\,\mathrm{V\,m^{-1}}$ due to high computational cost.

If the membrane voltage in one of the axon initial segments was higher than 60 mV, 0.2 ms after the stimulus, the event was described as activation; this is translated to spike propagation down the main axonal branch. At this point it is important to mention again that we use a reduced membrane voltage and consequently the resting potential was set to 0 mV.

For the computations, the angle steps for which the multicompartment models were tested were 15° and 10° for θ and ϕ respectively. Due to symmetry resulting from the formulas for calculating the extracellular potentials as stated in Equation 3.40, and because the models are projected on the two-dimensional plane (z coordinate is set to zero), the polar angle θ was within the range 0° - 90°. For the azimuthal angle ϕ the range 0° - 360° needed to be tested in order to cover the whole plane. However, for the linear case since the model was laid horizontally on the x axis, the range 0° - 180° for the azimuthal angle was sufficient for testing, due to rotational symmetry about the x axis.

5.2 Single Compartment Model

The threshold amplitude sufficient to generate an action potential during intracellular stimulation of the spherical soma with diameter 67 µm and for a duration of 1 ms was 2.3 nA when the calcium channel was used. This amplitude is slightly lower than the 2.5 nA needed when the calcium channel was omitted.

For the same current 2.5 nA, the maximum amplitude in both cases is almost the same, 44.26 mV when the T current was omitted, and 44.63 mV when the current was used. As we can see in Figure 5.1, when the Ca^{2+} channel is used, the spike precedes (in red) the action potential generated when the calcium channel is not active (in blue).

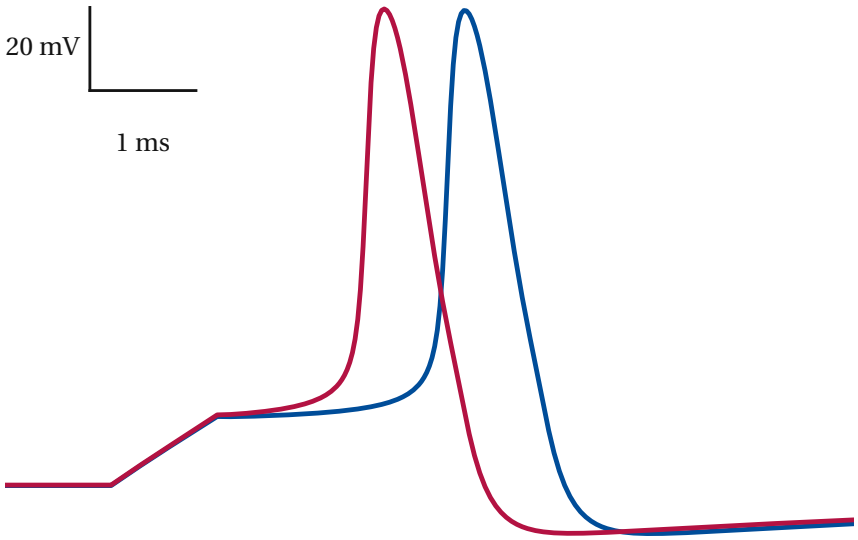

Figure 5.1: The single compartment model with (red) and without (blue) the T type current, for the same current pulse 2.5 nA.

For such a large spherical soma more current is required to change the voltage across the cell. The more realistic soma diameter used for the multicompartment models results in smaller threshold amplitudes, as we will see later.

Figure 5.2 shows that the activation of the Ca^{2+} channel (s gating variable) precedes the activation of the Na^{+} channel, which is still closed. This is in accordance with the known influence of this type of ion channel characterized as the 'first re-

sponder' to depolarization [4]. These types of channels have a low voltage threshold for activation that drives their opening in response to relatively small positive changes in membrane potential.

The sodium channel opens, driving the upstroke and the probability of the h variable which relates to the channel's inactivation state starts decreasing. Before it reaches its minimum, the slower potassium channel (n variable) opens and has its peak during repolarization.

The negative overshoot (hyperpolarization) after the action potential, is due to the slow deactivation of the potassium channel; potassium ions continue to exit, as they reach equilibrium when the membrane voltage is below -70 mV.

5.3 Multicompartment Models

5.3.1 Intracellular vs Extracellular Stimulation

For visualization purposes, only the longest branch of the dendritic and axonal processes has been used.

As shown in Table 5.1, injection in the middle of the dendrite results in higher threshold current than the current needed for stimulation at the dendritic end, both in the linear and 3D model. This happens because some extra current is needed for exciting the distal dendrite, in contrast to when stimulating the end.

In both models we observe that the most excitable part of the neuron is the axon terminal, whereas soma needs the more current for initiation of an action potential. In the linear model the axon terminal is more excitable even from the last node of Ranvier, which needs a slightly increased current 0.13 nA (not presented here) to elicit a spike.

During extracellular stimulation, as we see in table 5.2, the most excitable part of the cell for the linear case is the axon terminal, as observed in the intracellular stimulation. However, for the 3D model, the axon kink needs the least negative current to initiate a spike, compared to all the other locations tested. The axon terminal and other locations along the axon branch tested (not presented here) resulted in a more negative threshold for the 3D model. The dendritic end on the other hand has the highest threshold amplitude with $-14.5\,\mu$A.

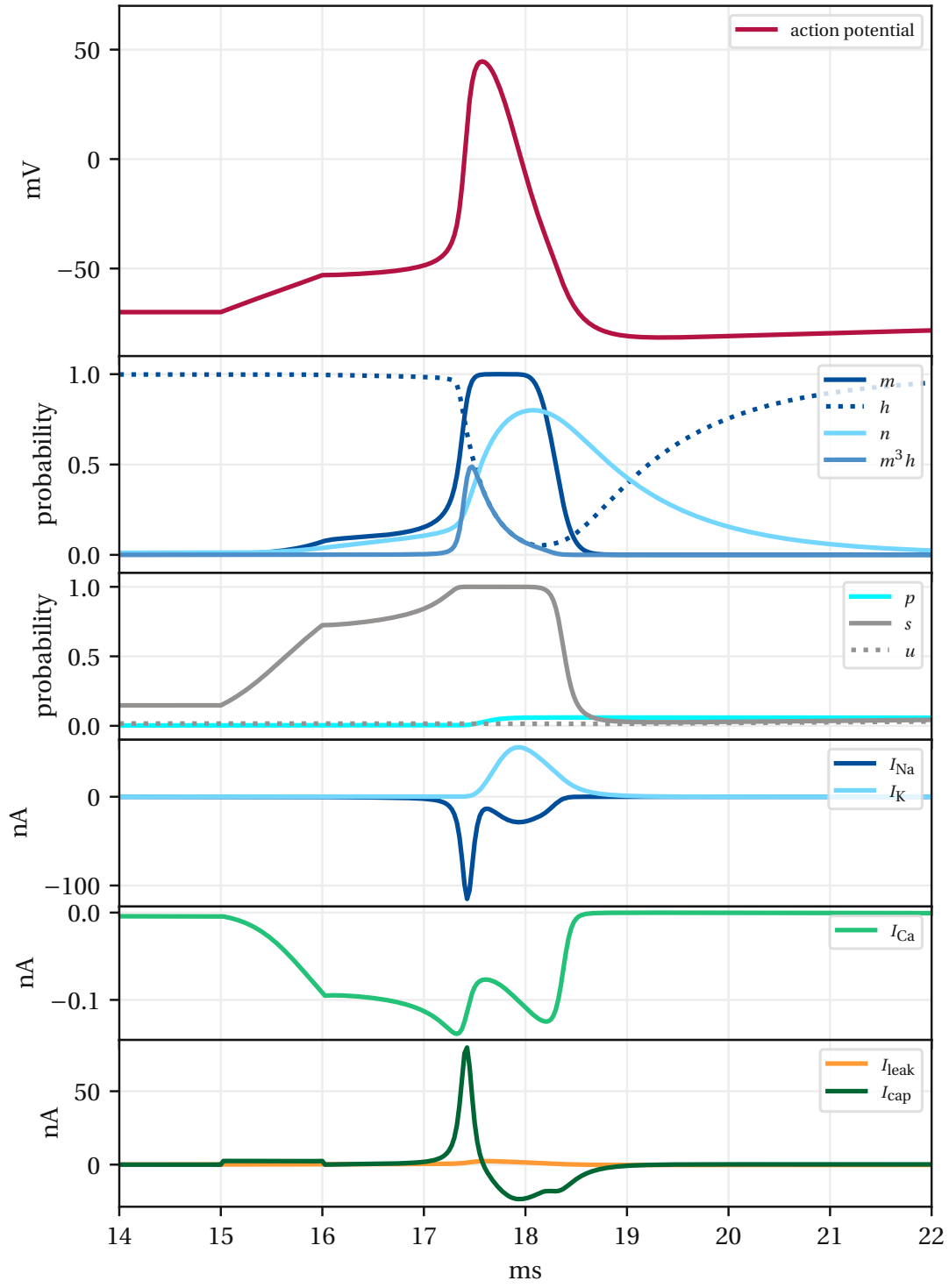

Figure 5.2: Intracellular stimulation of single compartment model with calcium channel, for a current pulse of 2.5 nA, duration of 1 ms and delay of 15 ms. The reason of the delayed stimulation was to ensure that the gating variables were in their steady state before stimulation, as the initialization of the gating variables in the `MOD` file was set to zero. Action potential generation can be seen in the top figure, and behavior of the gating variables in the two figures below. The calcium channel responds first upon depolarization (probability of s ascends upon stimulus), and then the opening of the sodium channel follows, indicated by an increase of the probability of m variable, and decrease of h (closure of inactivation gate). The potassium channel opens with a delay coinciding the closing of the inactivation gate of the sodium channel. Three figures on the bottom show the time course of the transmembrane currents influencing the membrane potential. The early inward sodium current drives the depolarization, whereas the delayed I_K shows the efflux of potassium ions. The fastest inward calcium current depicts the small, but essential influx of calcium ions. The capacitive current is zero when the action potential is at its maximum value.

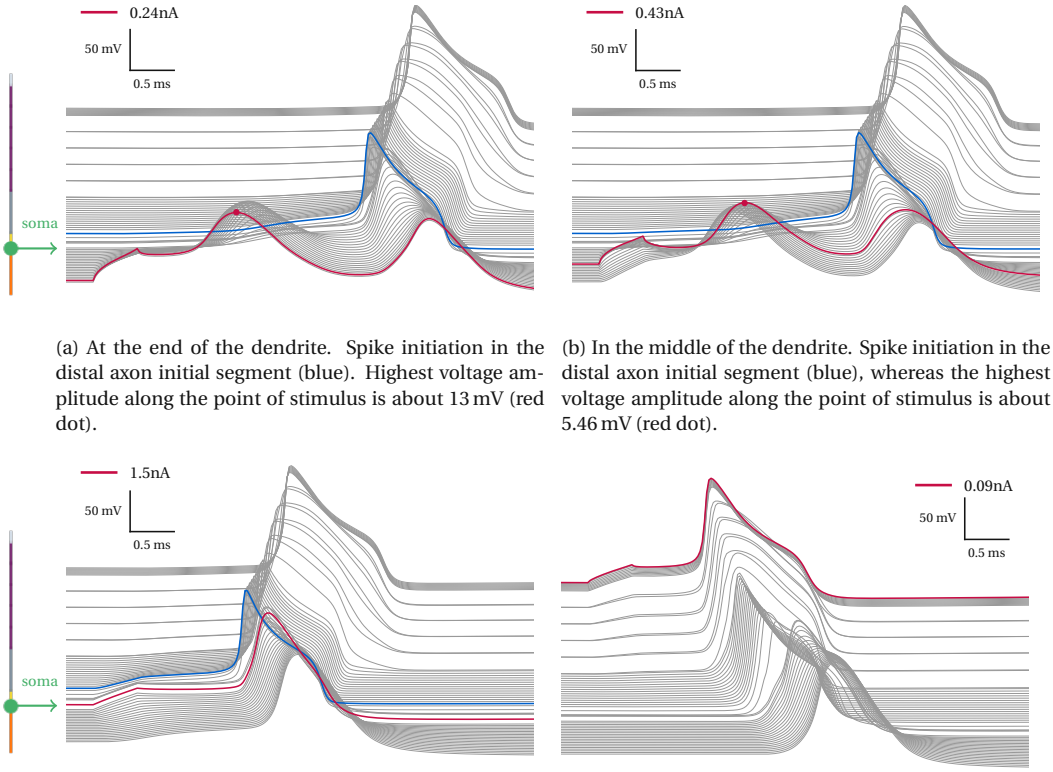

(a) At the end of the dendrite. Spike initiation in the distal axon initial segment (blue). Highest voltage amplitude along the point of stimulus is about 13 mV (red dot).

(b) In the middle of the dendrite. Spike initiation in the distal axon initial segment (blue), whereas the highest voltage amplitude along the point of stimulus is about 5.46 mV (red dot).

(c) In the soma. Spike initiation at the distal axon initial segment (blue).

(d) Axon terminal

Figure 5.3: Intracellular stimulation of the linear model in different locations (red), with corresponding threshold amplitudes.

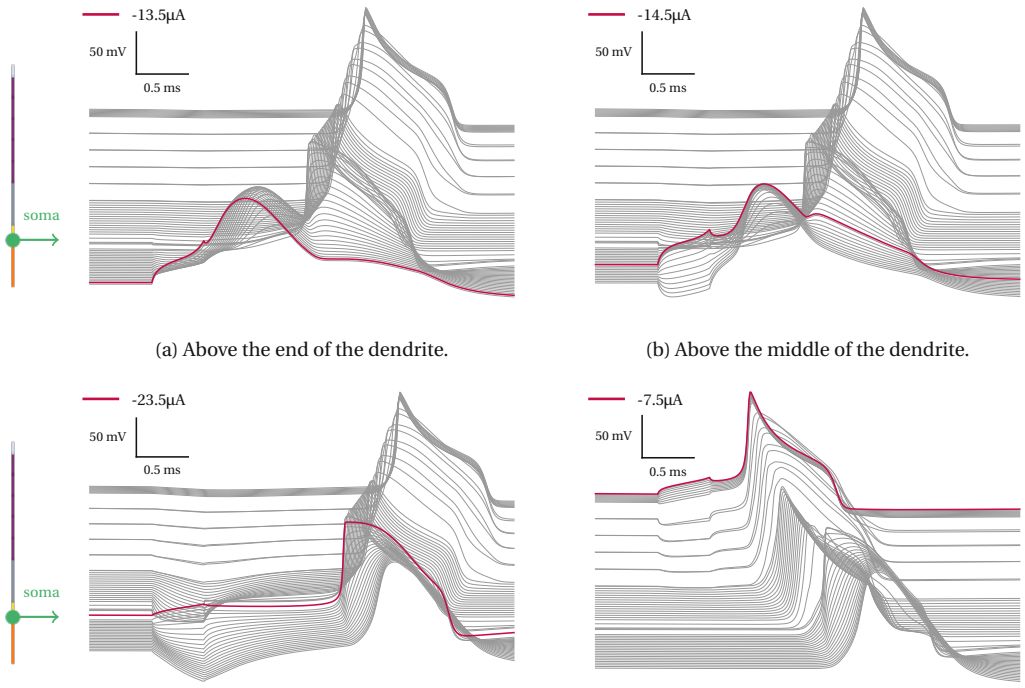

(a) Above the end of the dendrite.

(b) Above the middle of the dendrite.

(c) Above the soma.

(d) Above the axon terminal.

Figure 5.4: Extracellular stimulation of the linear model, 50 µm above the cell, with corresponding threshold amplitudes. Red lines correspond to the segment above which the stimulation was targeted.

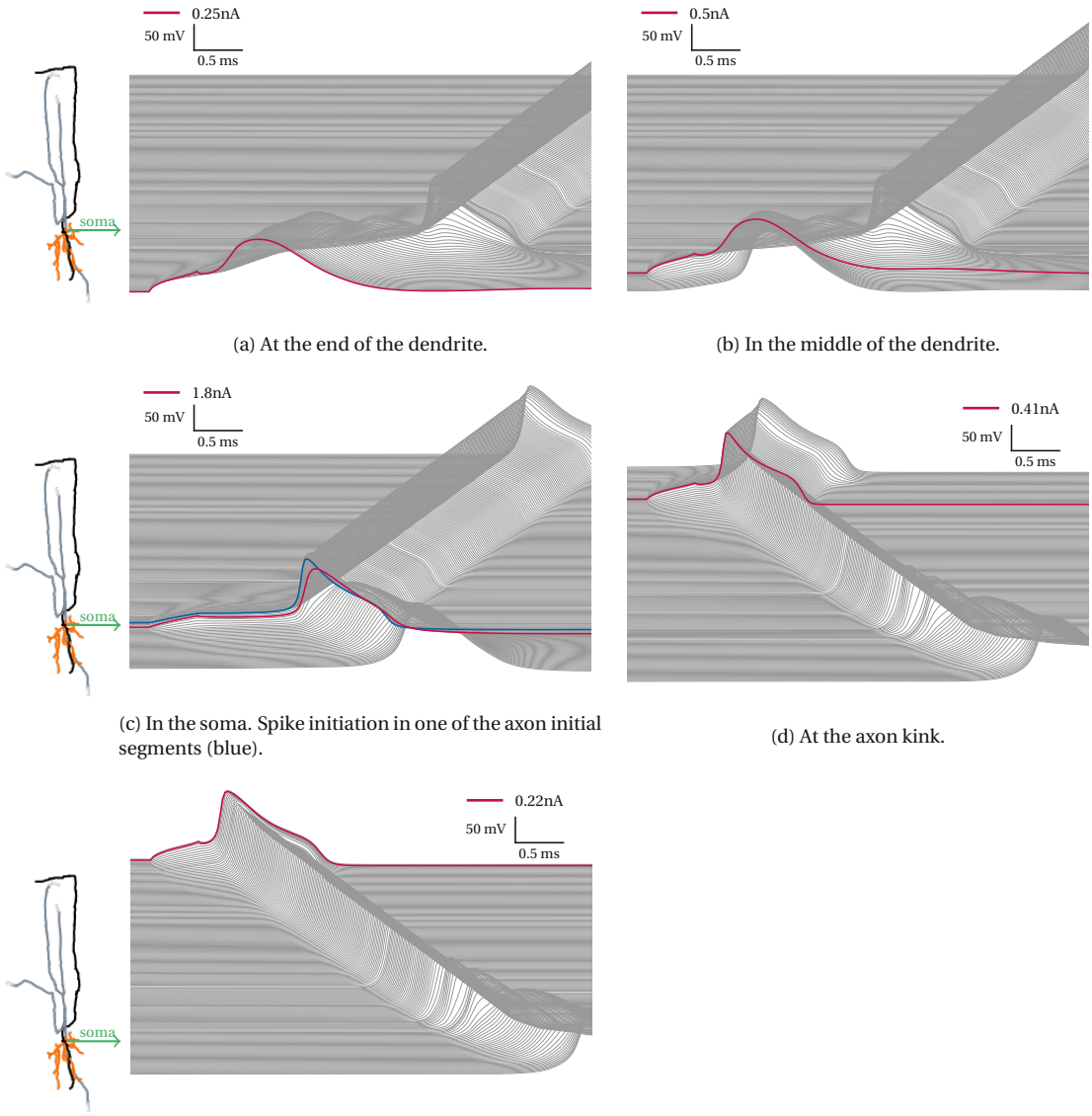

(a) At the end of the dendrite.

(b) In the middle of the dendrite.

(c) In the soma. Spike initiation in one of the axon initial segments (blue).

(d) At the axon kink.

(e) At the axon terminal.

Figure 5.5: Intracellular stimulation of 3D model in different locations (red), with corresponding threshold amplitudes. The path of the membrane potential visualized in the figures is only of the longest dendritic and axonal branches (black line in the 3D model on the left).

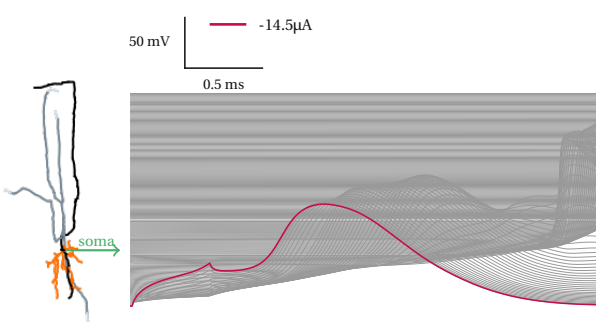

(a) Above the end of the dendrite.

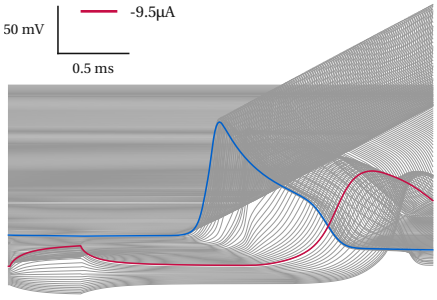

(b) Above the middle of the dendrite. An axonal segment (blue) is activated before the targeted dendrite.

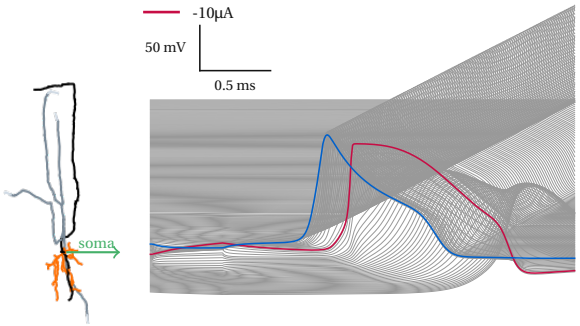

(c) Above the soma. Spike initiation in the axon initial segments (blue).

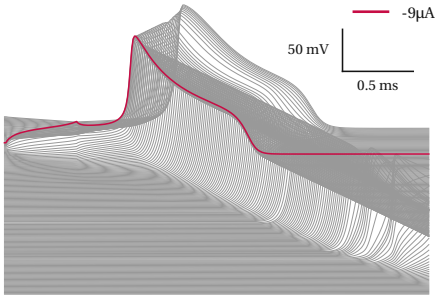

(d) Above the axon kink.

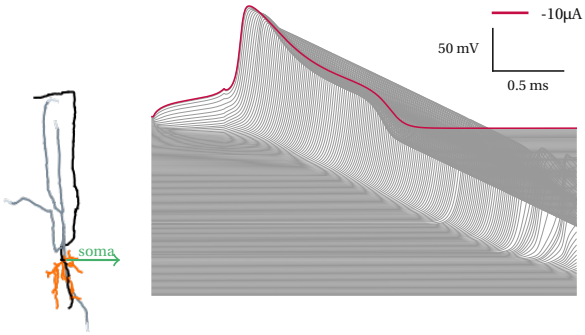

(e) Above the axon terminal.

Figure 5.6: Extracellular stimulation of 3D model 50 µm above the cell, in different locations, with corresponding threshold amplitudes. Red lines correspond to the segment above which the stimulation was targeted. The path of the membrane potential visualized in the figures is only of the longest dendritic and axonal branches (black line in the 3D model on the left).

The reason why the soma and the middle of the dendrite are easily excited with $-10\,\mu A$ and $-9.5\,\mu A$ respectively, can be explained by looking at the Figure 5.7. The electrode stimulates the cell in an area where the activating function f (3.43) is positive. This corresponds to an angle of 70.5°, with the electrode creating a circular region on the plane which separates the activated and deactivated parts of the cell. For these specific locations, the soma and the middle of the dendrite, the black circles in the Figure also include part of the axon initial segments (yellow) or the unmyelinated axon (grey) respectively. In reality axonal branches are stimulated as well. As a validation, an extra location was tested: stimulation above the middle of a dendrite that is close to no axon; in this case the threshold amplitude was even more negative at $-20\,\mu A$.

During somatic and dendritic intracellular stimulation of the linear model an axon initial segment is the site of spike initiation, as Figure 5.3 shows in a, b, c. Stimulation at the terminal results in initiation at the point of stimulus, as expected (d). Initiation at an axonal segment of the 3D model occurs during somatic and axonal intracellular stimulation (Figures 5.5c - 5.5e). For stimulation from a distance above the axon, first activation occurs at an axonal segment for stimulation above the middle of the dendrite (Figure 5.6b) and the soma (Figure 5.6c). For stimulation above the middle of the dendrite, the action potential is initiated at an axonal segment of the branch neighboring to the targeted dendrite. As we can see in Figure 5.7 stimulation above the middle of the dendrite activates a region that includes part of an axon. Consequently the axon of the visualized path will be activated before the targeted dendritic middle.

INTRACELLULAR STIMULATION

	Linear	3D
dendritic end	0.24	0.25
middle of dendrite	0.43	0.5
soma	1.5	1.8
axon kink		0.41
axon terminal	0.09	0.22

Table 5.1: Threshold currents in nA for stimulus duration 0.5 ms.

By omitting the T type calcium channel dendritic stimulation of the linear model

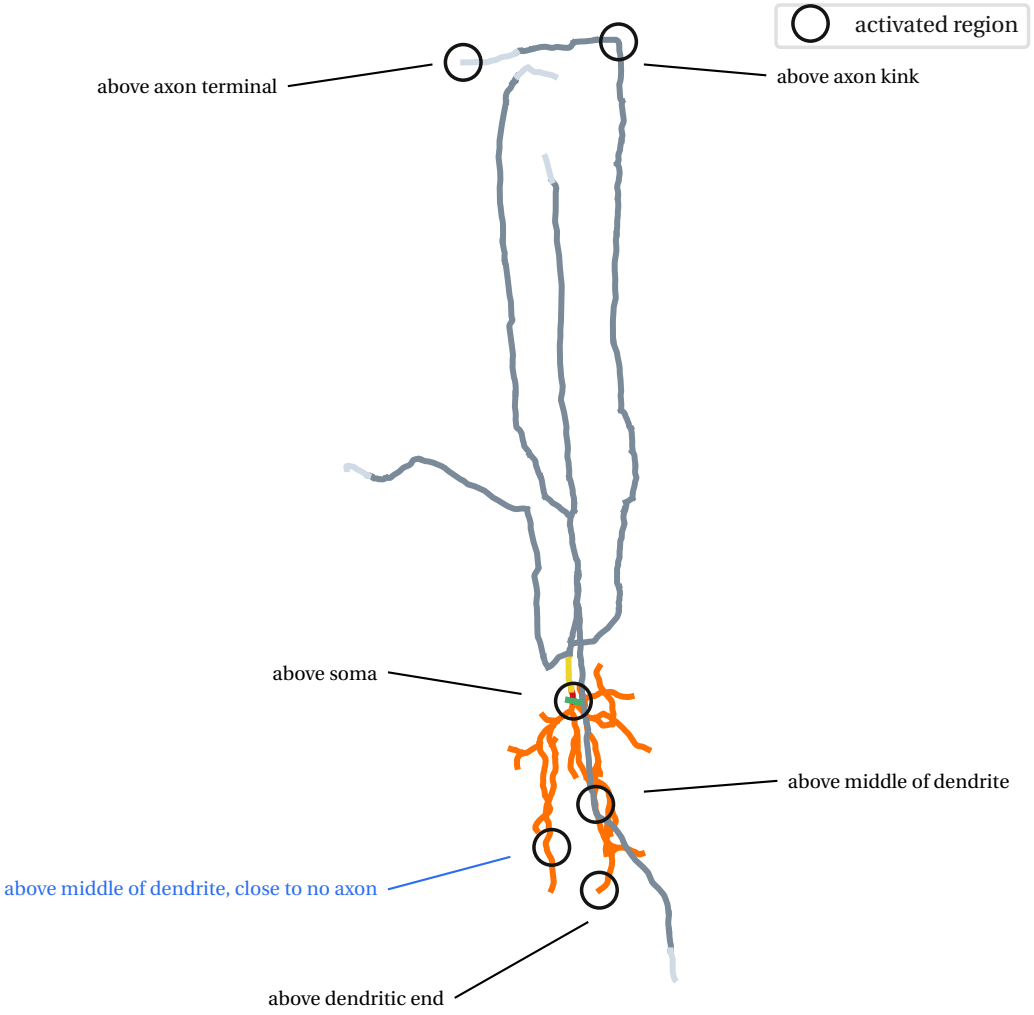

Figure 5.7: Activated regions (black circles) during extracellular stimulation above different locations in the 3D model. In order to test the excitation of the dendrite, an extra stimulus location that is not close to any axonal branch was used, as shown in light blue.

EXTRACELLULAR STIMULATION

	Linear	3D
dendritic end	-13.5	-14.5
middle of dendrite	-14.5	-9.5
soma	-23.5	-10
axon kink		-9
axon terminal	-7.5	-10

Table 5.2: Threshold currents in μA for stimulus duration 0.5 ms.

could not result in a propagating spike. Furthermore the action potential was delayed during somatic stimulation. For the 3D model slightly higher threshold current amplitudes were observed.

Passive axon terminals

By modeling the axon terminal of the linear model as a passive membrane, stimulation in the same position results in a less sharp action potential shape at these processes, as well as to reduced maximum amplitude. This difference reaches the 9 mV compared to the simulation with original densities, as stated in the Table 4.4 (Figure 5.8a). Threshold current amplitude of the passive axonal terminal is more than double at 0.2 nA, compared to the active terminal at 0.09 nA.

Similarly, in the case of the 3D model, stimulation at the passive axonal terminal, the shape of the action potential changes at the last compartments and the threshold amplitude is doubled (Figure 5.8b).

There is no effect on the threshold current at any other location site of the linear or 3D model.

Effects of a large soma

As mentioned in the beginning of the chapter, as well as in 4.2.1, the soma diameter had to be reduced to 30 μm. In Figure 4.2 we saw that intracellular dendritic stimulation of the linear model resulted in non propagating action potentials for the initially big soma of the single compartment model.

We did additional tests using the initial large soma of the single compartment

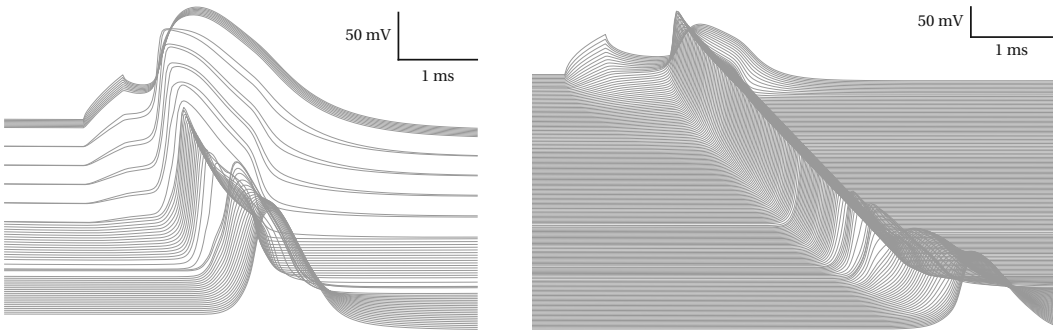

(a) Linear model.

(b) 3D model.

Figure 5.8: Intracellular stimulation at the axonal end with passive axon terminals. Lines on the bottom correspond to the dendrite of the models, lines on the top are the passive axonal processes.

model (diameter of 67 µm) in order to investigate the effect of its diameter on our results.

For the linear model, threshold amplitudes of stimulations inside and outside of the spherical soma were tripled. For axonal stimulation no changes were observed.

Intracellular stimulation of the axon and soma of the three-dimensional model activated the cell. For the latter, increased threshold current amplitude was observed, as well as a delay of the spike at the somatic segments. The results of stimulation 50 µm above the branched neuron remained unchanged: extracellular stimulation activated the cell for all points tested and for the same threshold amplitudes as when the reduced soma diameter was used.

In all stimulations of both models, the site of action potential initiation was independent of the soma diameter deployed in the simulations.

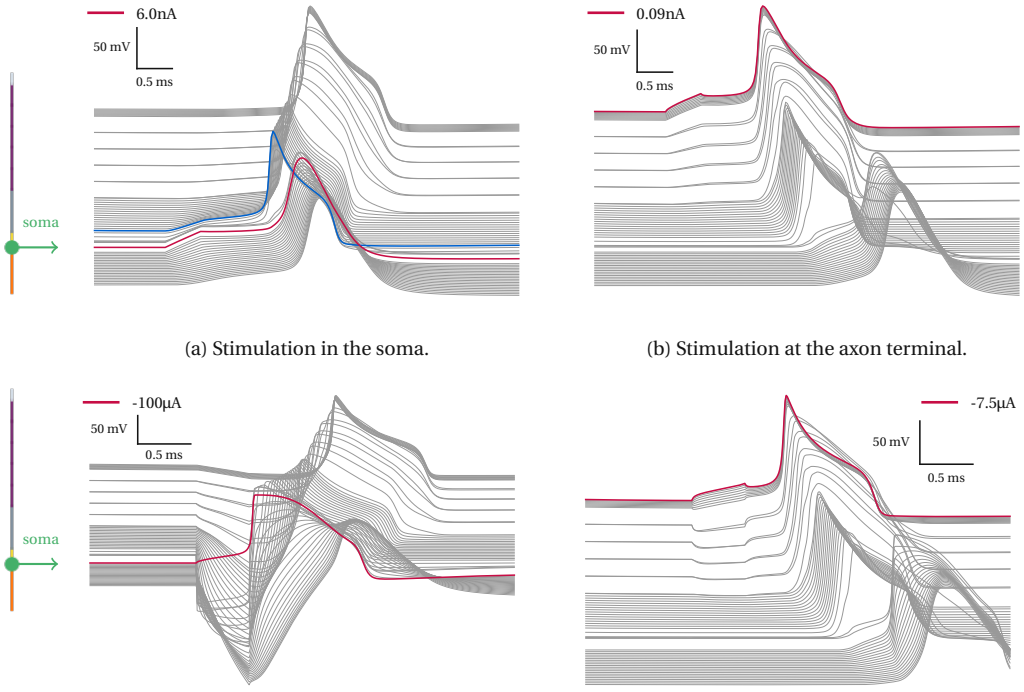

(a) Stimulation in the soma.

(b) Stimulation at the axon terminal.

(c) Stimulation above the soma.

(d) Stimulation above the axon terminal.

Figure 5.9: Stimulation of the linear model with original soma diameter of 67 µm at locations that resulted in the generation of an action potential. Red lines correspond to the targeted point of stimulus and blue lines to spike initiation at an axonal segment.

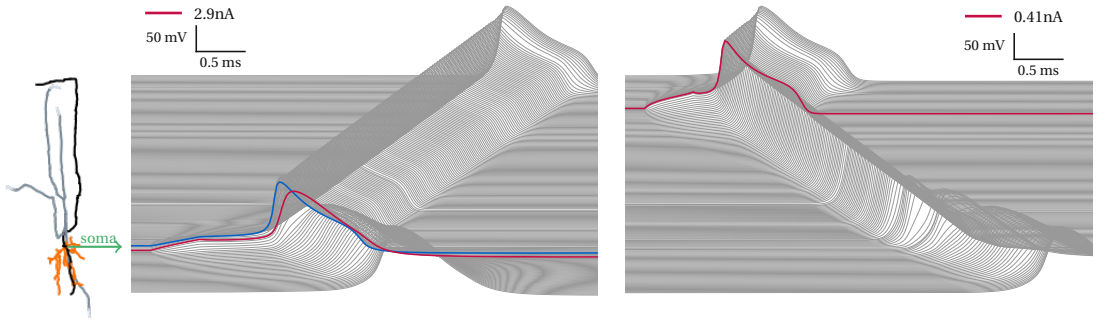

(a) Stimulation in the soma.

(b) Stimulation at the axon kink.

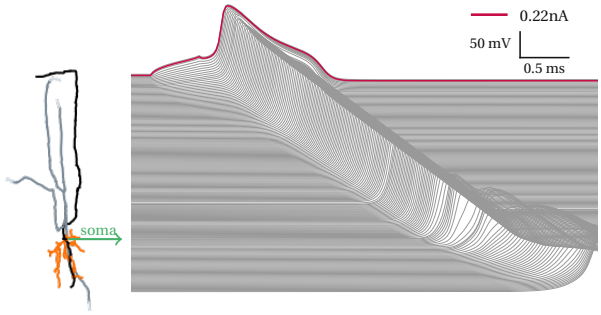

(c) Stimulation at the axon terminal.

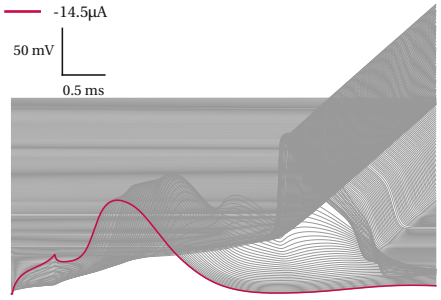

(d) Stimulation above the dendritic end.

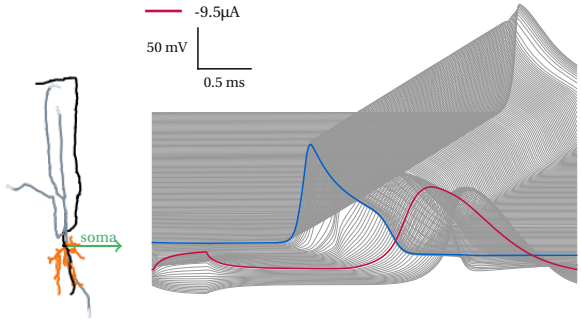

(e) Stimulation above the middle of the dendrite.

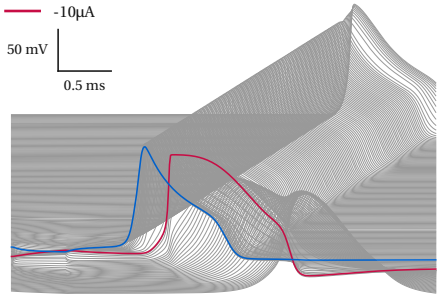

(f) Stimulation above the soma.

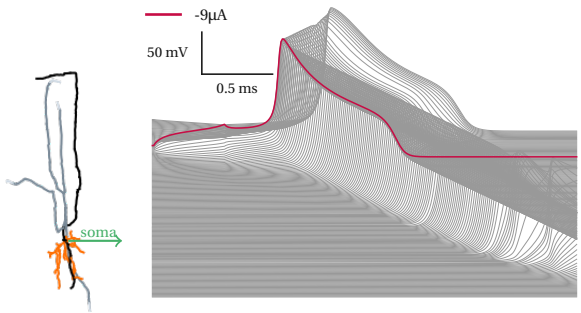

(g) Stimulation above the axon kink.

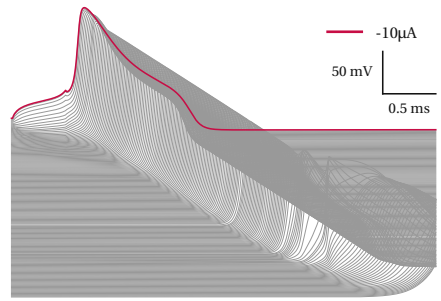

(h) Stimulation above the axon terminal.

Figure 5.10: Stimulation of the 3D model with original soma diameter of 67 µm at locations that resulted in the generation of an action potential. Red lines correspond to the targeted point of stimulus and blue lines to spike initiation at an axonal segment.

5.3.2 Transcranial Magnetic Stimulation

During transcranial electric and magnetic stimulation, the local field generated can be simulated using a uniform electric field (E-field) [1].

The method used is similar to the process used for modeling the extracellular stimulation 50 µm above the cell, as described in the previous chapter. However now the extracellular potential generated is due to the E-field, measured in $\mathrm{V\,m^{-1}}$, as described in 3.40.

The binary search algorithm was used for a stimulus duration of 0.025 ms, for finding the minimum E-field strength, strong enough to result in a spike generation.

As we can see in Figure 5.11 upward ($\theta = 0°$) uniform E-fields are not able to excite the linear model, for the maximum threshold amplitude tested.

We notice that E-fields perpendicular, or almost perpendicular to the model do not result in an action potential, since our model is linear, with no branches. Therefore a polar angle of 15° results in maximum thresholds, for the azimuthal angles that depolarize the neuron sufficiently enough to elicit an action potential. In this case excitation is impossible for azimuthal angles in the window 50°-100°, as this orientation is again almost perpendicular to the linear model. Detailed threshold amplitudes can be found in Table 5.3.

The model is easily excitable for polar angles greater then 45° and azimuthal angles for which the E-fields is not vertical. Consequently, minimum thresholds are observed for E-fields aligned with the model, and with an orientation heading from the dendrite toward the axon terminal.

Analogous results are presented in the reference publication of [1]. The simpler model has a straight axon, to which a fairly branched dendrite has been added. The maximal threshold for the straight axon model achieved for E-fields perpendicular to the somatodendritic axis. The threshold minimized when the E-field aligned with the straight axon and oriented from the dendrite down the axon.

For a better understanding, the heatmap shown in Figure 5.11 is visualized in the three-dimensional space (Figure 5.13), by filling the threshold amplitudes of the missing azimuthal and polar angle pairs, due to axial symmetry.

Similarly to the realistic model in [1], our 3D model shows less variability in the threshold amplitudes among the θ and ϕ angle pairs. On the contrary the simple

models are much more sensitive to the changes in the E-field directions, since they only have one axonal terminal capable of activation.

Moreover, upward E-fields were not able to activate the branched neuron which is projected onto the two-dimensional plane. A polar angle of 15° resulted in highest thresholds across the azimuthal angles, as Figure 5.12 and Table 5.4 show. Minimum threshold amplitude is observed for orientations aligned with the axon ($\theta = 90°$, $\phi = 100°$, 270° and 280°). In Figure 5.14 we can see the threshold amplitudes mapped in a sphere in relation to the three-dimensional model.

The presented results show E-field threshold amplitudes normalized to minimum.

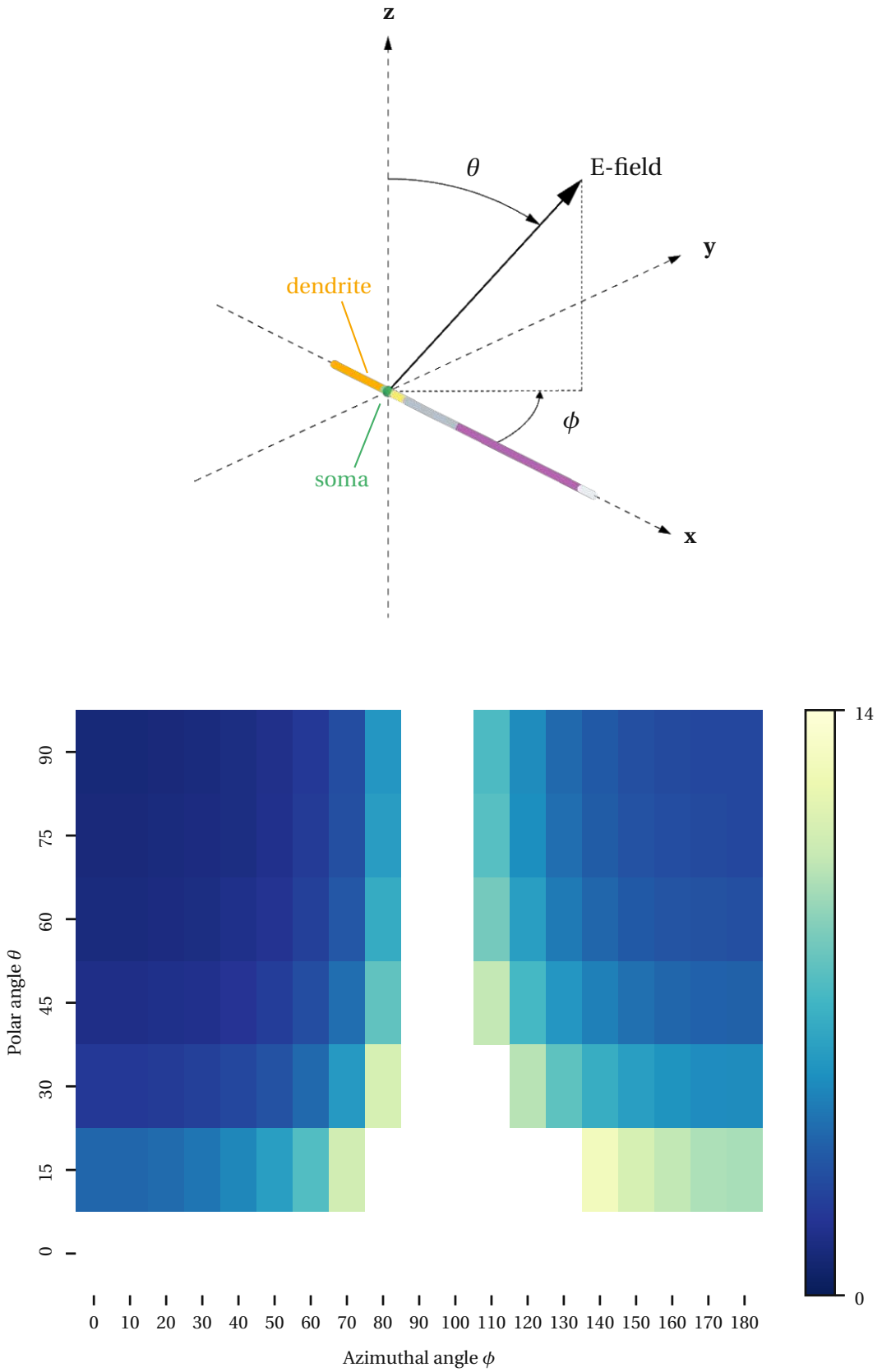

Figure 5.11: Figure on the **top** shows the orientation of the linear model. The heatmap on the **bottom** shows the E-field thresholds in Vm^{-1} for the polar and azimuthal pairs tested. Perpendicular E-fields cannot activate the cell.

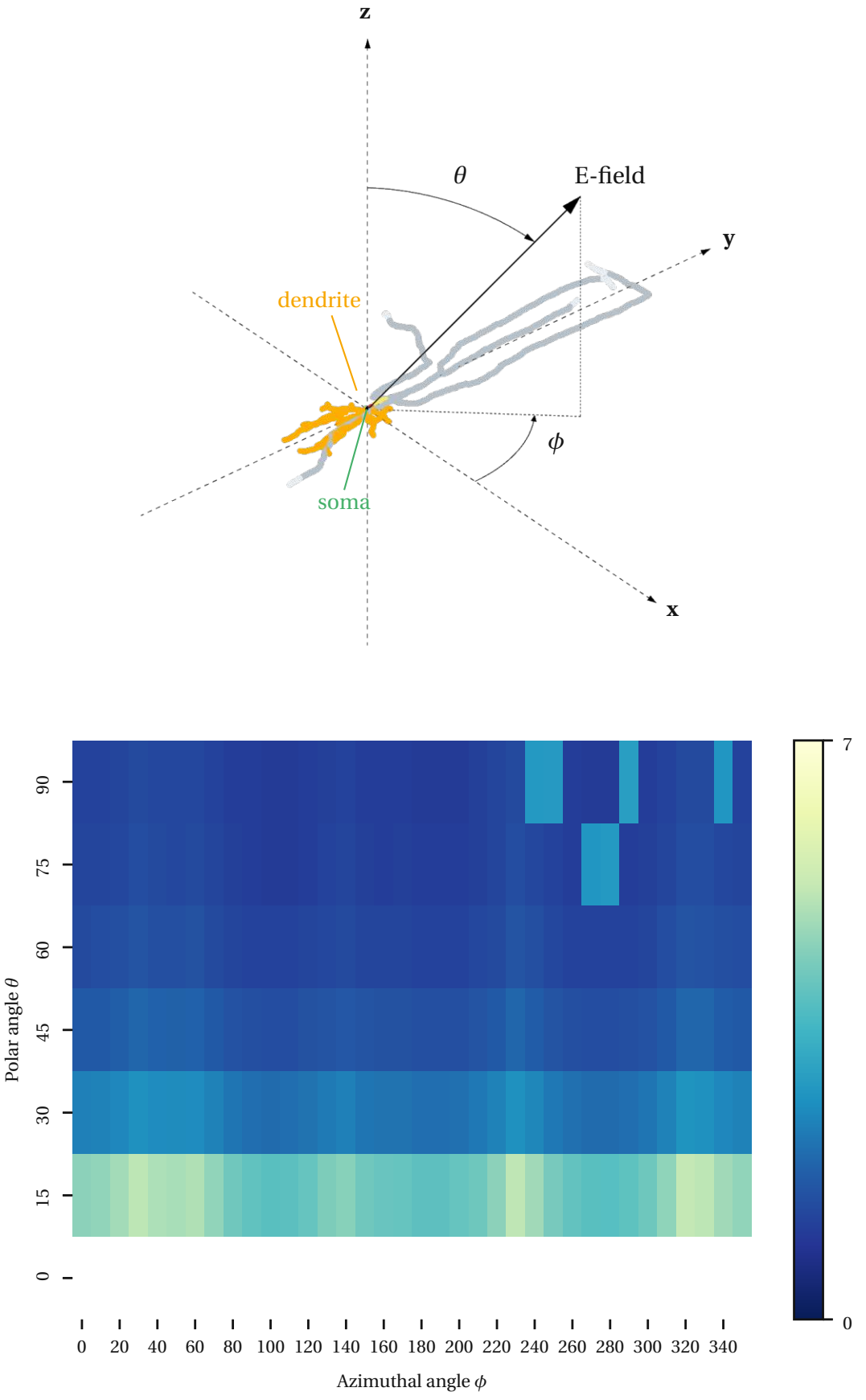

Figure 5.12: Figure on the **top** shows the orientation of the 3D model. The heatmap **below** shows the E-field thresholds in Vm^{-1} for the polar and azimuthal pairs tested. For a zero polar angle (upward E-field) the stimulation did not result in activation.

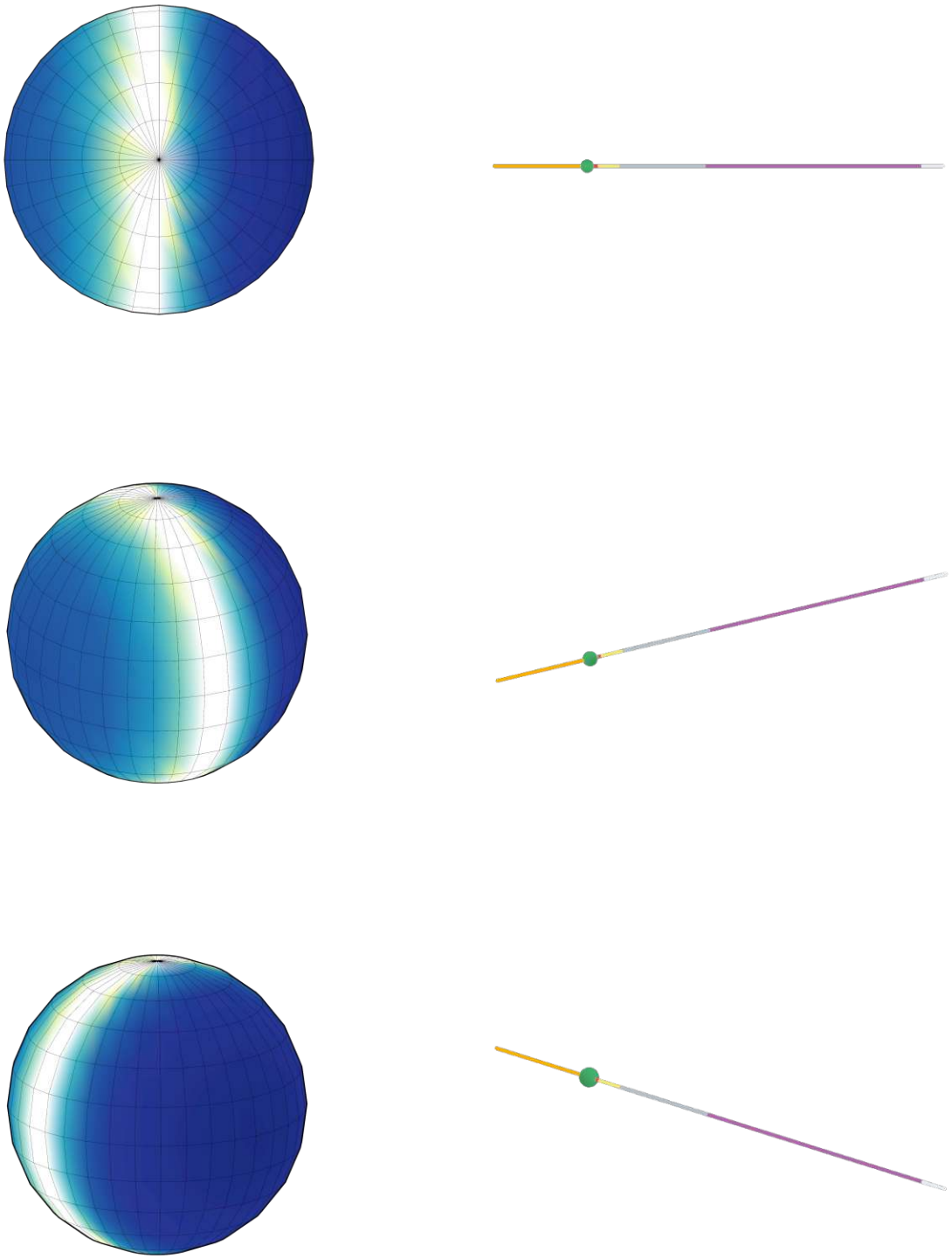

Figure 5.13: 3D representation of the threshold amplitudes for the different E-field orientations in relation to the linear model. The sphere shows the different azimuthal-polar angle pairs for which the transcranial magnetic stimulation results in the generation of an action potential. The values of the E-field amplitude is given by the colorbar as in Figure 5.11.

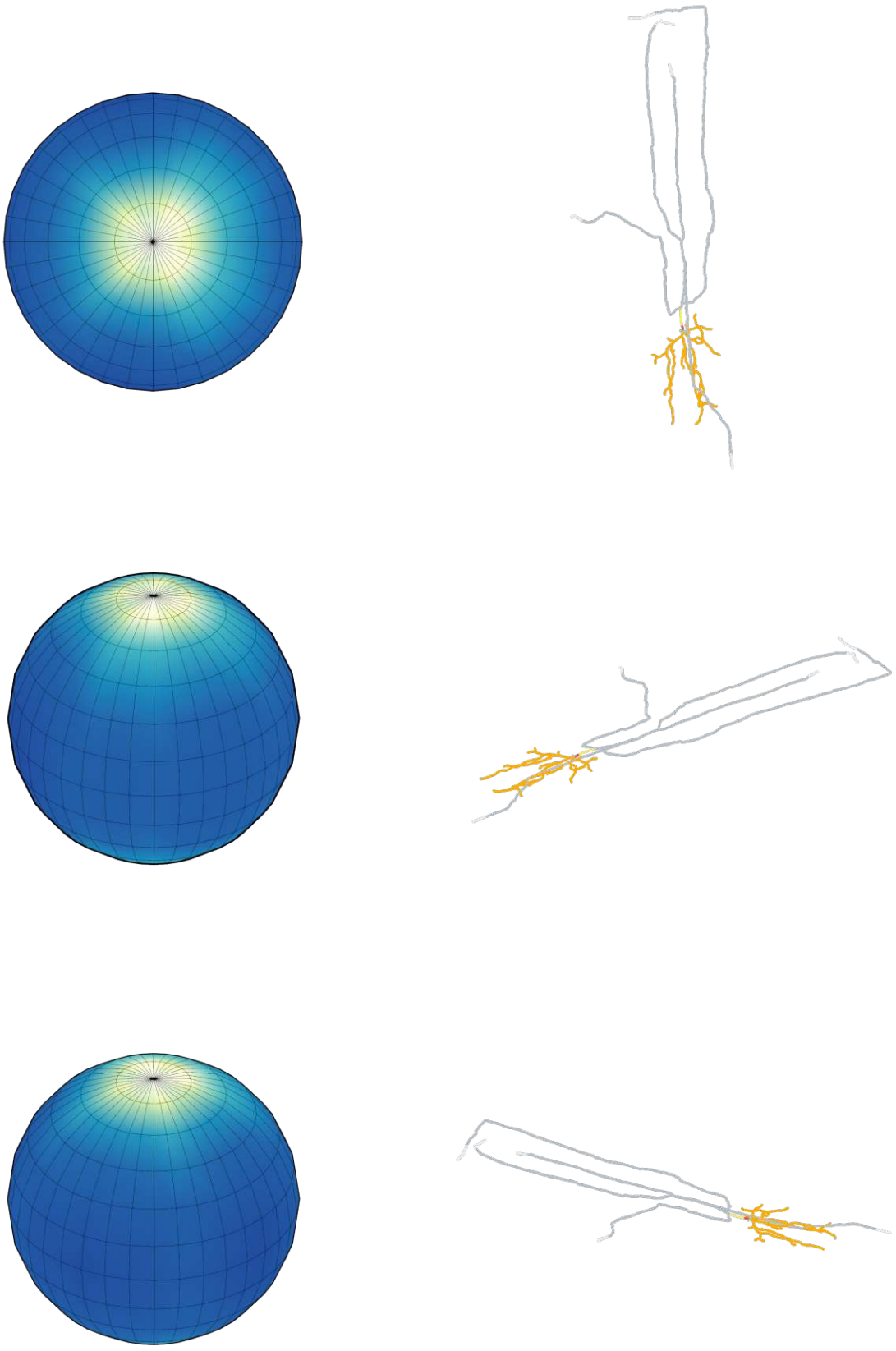

Figure 5.14: 3D sphere in relation to the 3D model for different angles. The sphere shows the different azimuthal-polar angle pairs for which the transcranial magnetic stimulation results in the generation of an action potential. The values of the E-field amplitude is given by the colorbar as in Figure 5.12.

E-field threshold amplitudes of the linear model

ϕ \ θ	0°	15°	30°	45°	60°	75°	90°
0°	-	3.86	2	1.41	1.15	1.04	1
10°	-	3.92	2.03	1.44	1.17	1.05	1.02
20°	-	4.11	2.13	1.5	1.23	1.1	1.06
30°	-	4.46	2.31	1.63	1.33	1.2	1.15
40°	-	5.04	2.61	1.85	1.51	1.35	1.31
50°	-	6.01	3.11	2.2	1.8	1.61	1.56
60°	-	7.73	4	2.83	2.31	2.07	2
70°	-	11.3	5.85	4.13	3.38	3.03	2.92
80°	-	-	11.5	8.14	6.65	5.96	5.76
90°	-	-	-	-	-	-	-
100°	-	-	-	-	-	-	-
110°	-	-	-	10.8	8.8	7.89	7.62
120°	-	-	10.4	7.37	6.02	5.39	5.21
130°	-	-	8.11	5.73	4.68	4.2	4.05
140°	-	13.1	6.8	4.81	3.93	3.52	3.4
150°	-	11.6	6.02	4.25	3.47	3.11	3.01
160°	-	10.7	5.55	3.92	3.2	2.87	2.77
170°	-	10.2	5.29	3.74	3.06	2.74	2.65
180°	-	10.1	5.21	3.68	3.01	2.7	2.61
190°	-	10.2	5.29	3.74	3.06	2.74	2.65
200°	-	10.7	5.55	3.92	3.2	2.87	2.77
210°	-	11.6	6.02	4.25	3.47	3.11	3.01
220°	-	13.1	6.8	4.81	3.93	3.52	3.4
230°	-	-	8.11	5.73	4.68	4.2	4.05
240°	-	-	10.4	7.37	6.02	5.39	5.21
250°	-	-	-	10.8	8.8	7.89	7.62
260°	-	-	-	-	-	-	-
270°	-	-	-	-	-	-	-
280°	-	-	11.5	8.14	6.65	5.96	5.76
290°	-	11.3	5.85	4.13	3.38	3.03	2.92
300°	-	7.73	4	2.83	2.31	2.07	2
310°	-	6.01	3.11	2.2	1.8	1.61	1.56
320°	-	5.04	2.61	1.85	1.51	1.35	1.31
330°	-	4.46	2.31	1.63	1.33	1.2	1.15
340°	-	4.11	2.13	1.5	1.23	1.1	1.06
350°	-	3.92	2.03	1.44	1.17	1.05	1.02

Table 5.3: E-field threshold amplitudes of the linear model normalized to minimum and rounded to 3 significant figures. The angle pairs tested were in the polar range 0° - 90° and azimuthal range 0° - 180°. The rest azimuthal angles are derived from axial symmetry. Every column shows the thresholds for the whole $x-y$ plane for a specific polar angle θ. Dashes represent orientations that did not result in neuronal activation.

E-field threshold amplitudes of the 3D model

ϕ \ θ	0°	15°	30°	45°	60°	75°	90°
0°	-	4.52	2.34	1.66	1.35	1.21	1.17
10°	-	4.59	2.38	1.69	1.37	1.23	1.19
20°	-	4.8	2.48	1.75	1.43	1.28	1.24
30°	-	5.13	2.65	1.88	1.53	1.37	1.33
40°	-	4.93	2.55	1.81	1.47	1.32	1.3
50°	-	4.88	2.52	1.79	1.46	1.31	1.26
60°	-	4.96	2.57	1.82	1.49	1.33	1.3
70°	-	4.58	2.37	1.67	1.37	1.23	1.19
80°	-	4.17	2.16	1.53	1.25	1.12	1.09
90°	-	3.95	2.04	1.45	1.18	1.06	1.04
100°	-	3.85	1.99	1.41	1.15	1.03	1
110°	-	3.88	2.01	1.42	1.16	1.04	1.02
120°	-	4.03	2.09	1.49	1.2	1.08	1.04
130°	-	4.33	2.24	1.58	1.29	1.17	1.12
140°	-	4.47	2.31	1.63	1.33	1.21	1.16
150°	-	4.18	2.17	1.53	1.25	1.12	1.08
160°	-	4.05	2.1	1.49	1.22	1.09	1.06
170°	-	4.04	2.09	1.48	1.21	1.1	1.05
180°	-	3.91	2.02	1.43	1.17	1.05	1.01
190°	-	3.9	2.02	1.43	1.16	1.05	1.01
200°	-	4	2.07	1.47	1.2	1.09	1.04
210°	-	4.13	2.19	1.55	1.27	1.14	1.1
220°	-	4.52	2.36	1.67	1.35	1.26	1.21
230°	-	5.16	2.67	1.89	1.54	1.38	1.34
240°	-	4.77	2.46	1.74	1.42	1.28	2.81
250°	-	4.27	2.21	1.56	1.28	1.15	2.83
260°	-	3.98	2.06	1.46	1.2	1.09	1.04
270°	-	3.84	1.99	1.41	1.16	2.74	1
280°	-	3.82	1.98	1.4	1.16	2.81	1
290°	-	3.92	2.03	1.43	1.18	1.06	2.91
300°	-	4.14	2.15	1.53	1.26	1.13	1.09
310°	-	4.55	2.35	1.67	1.37	1.23	1.19
320°	-	5.22	2.7	1.91	1.57	1.4	1.36
330°	-	5.12	2.65	1.88	1.53	1.38	1.34
340°	-	4.76	2.47	1.74	1.43	1.3	2.74
350°	-	4.59	2.37	1.68	1.37	1.23	1.19

Table 5.4: E-field threshold amplitudes of the 3D model normalized to minimum and rounded to 3 significant figures. The angle pairs tested were in the polar range 0° - 90° and azimuthal range 0° - 360°. Every column shows the thresholds for the whole $x-y$ plane for a specific polar angle θ. Dashes represent orientations that did not result in neuronal activation.

Action potential initiation site

Action potentials were not initiated at the soma or axon initial segments of the linear model, for none of the tested orientations. In slightly more than half of the cases, the action potential generated at a segment of the axon terminal. For the rest, dendritic initiation was observed. This is in agreement with the fact that in uniform E-fields depolarization is predicted to occur only at geometrically discontinuous sites, such as terminations [1]. Moreover, axon terminals indeed experienced the greatest polarization, resulting in increased voltage amplitudes during the spikes.

Furthermore, the smallest threshold amplitude observed resulted in a spike with initiation site at the axon terminal of the linear model.

Similarly to the linear model, for the three-dimensional model no spike initiated at the soma or the axon initial segments. In 86% of the cases the action potential generated at an axon terminal, and in only 10% at an unmyelinated axon. Exactly three segments of two distinct dendritic branches were the site of initiation in just 6 cases. All these dendritic segments constitute sites of bending or are very close to a morphological discontinuity.

The initiation sites of the minimum and maximum thresholds with corresponding membrane potentials in different processes of the 3D neuron can be seen in Figure 5.15.

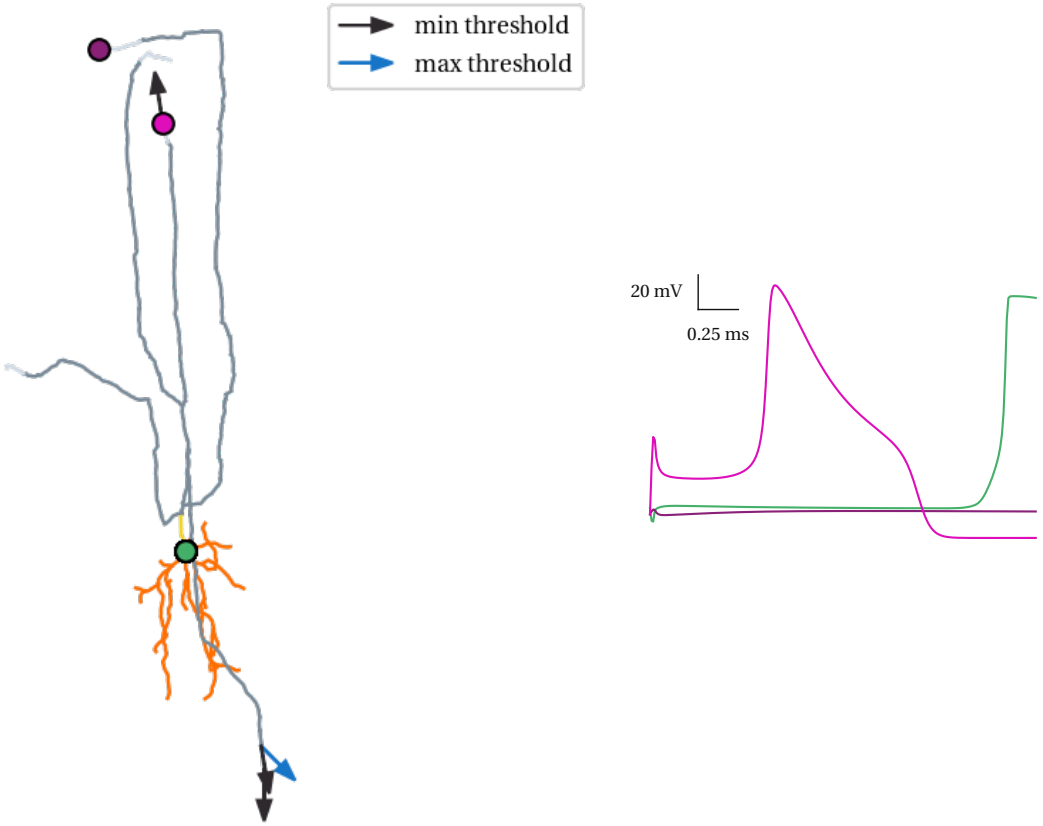

Figure 5.15: **Left**: Orientation of E-field for the minimum and maximum threshold amplitudes that could elicit an action potential. The positioning of the arrows correspond to the action potential initiation sites, which are the axon terminals of two axonal branches. **Right**: Membrane potential recordings with E-field direction indicated by the black arrow heading upwards, as shown in the left Figure. The recordings are from the first activated axon terminal (magenta), indirectly activated soma (green) and axon terminal of the longest axonal branch (dark purple), as the filled circles show in the left figure.

Chapter 6

Conclusion

For this thesis two neuron models were simulated in order to study the effects of different types of stimulation on them, generated by current injection and magnetic induction. In all cases the goal was to investigate the excitability of the models, by finding the minimum threshold amplitude that results in the generation of an action potential.

Intracellular stimulation of the linear model results in action potential initiation at an axonal segment for all stimulation locations. We observe the exact opposite for stimulation from a distance.

In the 3D model, dendritic stimulation leads to spike generation at the point of stimulus, during stimulation inside the cell. Initiation site during extracellular stimulation of the branched model occurs at an axonal segment in all but one cases: above the end of the dendrite.

When the models are subjected to magnetic stimulation the smallest threshold amplitude is achieved when the E-field is aligned with the axon: in particular the E-field is oriented from the dendrite toward the axon terminal. In the three-dimensional case, the direction is from a dendritic branch to one of the axonal terminals as shown in Figure 5.15.

For the minimum E-field threshold amplitudes the axon terminal is the neuronal process activated first in both models.

6.1 Limitations

Due to lack of electrophysiological data on Martinotti cells we adjusted the conductances of the single compartment neurons as described in [32] for simulating the somatodendritic segments of our linear and three-dimensional multicompartment models. For the axon the biophysics of the model described in [50] were used.

For a better understanding of the behavior of Martinotti cells further experimental studies are necessary. Additional computational studies with a higher degree of axonal branching and arborization, as well as implementation of myelination in the three-dimensional model can help investigate the dependence of the aforementioned characteristics in neuron polarization.

Bibliography

[1] A. S. Aberra, A. V. Peterchev, and W. M. Grill. Biophysically realistic neuron models for simulation of cortical stimulation. *Journal of Neural Engineering*, 15(6), 10 2018.

[2] B. Alberts, A. Johnson, J. Lewis, M. Raff, K. Roberts, and P. Walter. Ion Channels and the Electrical Properties of Membranes. 2002.

[3] BioRender. Patch-Clamp Recording Principle.

[4] S. M. Cain and T. P. Snutch. Contributions of T-type calcium channel isoforms to neuronal firing. *Channels*, 4(6):475, 2010.

[5] J. H. Caldwell, K. L. Schaller, R. S. Lasher, E. Peles, and S. R. Levinson. Sodium channel Nav1.6 is localized at nodes of Ranvier, dendrites, and synapses. *Proceedings of the National Academy of Sciences of the United States of America*, 97(10):5616–5620, 5 2000.

[6] N. T. Carnevale and M. L. Hines. *The NEURON book*. Cambridge University Press, 1 2006.

[7] R. Chen. Psychostimulants, Brain Membrane Lipids and Dopamine Transmission. *Journal of Biomolecular Research & Therapeutics*, 5(2), 2016.

[8] S. Y. Chiu, J. M. Ritchie, R. B. Rogart, and D. Stagg. A quantitative description of membrane currents in rabbit myelinated nerve. *The Journal of Physiology*, 292(1):149–166, 7 1979.

[9] I. Cobos, M. E. Calcagnotto, A. J. Vilaythong, M. T. Thwin, J. L. Noebels, S. C. Baraban, and J. L. Rubenstein. Mice lacking Dlx1 show subtype-specific loss of

interneurons, reduced inhibition and epilepsy. *Nature Neuroscience*, 8(8):1059–1068, 8 2005.

[10] R. B. Colquitt, D. A. Colquhoun, and R. H. Thiele. In silico modelling of physiologic systems, 2011.

[11] G. M. Cooper. Cell Membranes. 2000.

[12] D. F. L. C. K. A.-S. L. J. O. M. Dale Purves, George J Augustine and S. M. Williams., editors. *Neuroscience - NCBI Bookshelf*.

[13] G. N. Elston. Specialization of the neocortical pyramidal cell during primate evolution. In *Evolution of Nervous Systems*, volume 4, pages 191–242. Elsevier Inc., 1 2007.

[14] J. Fernandes. ALS Cell Therapies May Benefit from Study of Motor Neuron Formation.

[15] M. Flint Beal, R. A. Clevens, and M. F. Mazurek. Somatostatin and neuropeptide Y immunoreactivity in parkinson's disease dementia with alzheimer's changes. *Synapse*, 2(4):463–467, 1988.

[16] B. Frankenhaeuser. Sodium permeability in toad nerve and in squid nerve. *The Journal of Physiology*, 152(1):159, 6 1960.

[17] F. Fregni and A. Pascual-Leone. Technology Insight: Noninvasive brain stimulation in neurology - Perspectives on the therapeutic potential of rTMS and tDCS, 7 2007.

[18] F. Fröhlich. Microcircuits of the Neocortex. In *Network Neuroscience*, pages 85–95. Elsevier, 1 2016.

[19] K. J. Gingrich and J. Yang. Molecular physiology. In *Foundations of Anesthesia*, pages 79–89. Elsevier Ltd, 1 2006.

[20] J. H. Goldberg, C. O. Lacefield, and R. Yuste. Global dendritic calcium spikes in mouse layer 5 low threshold spiking interneurones: Implications for control of pyramidal cell bursting. *Journal of Physiology*, 558(2):465–478, 7 2004.

[21] H. Gray. *Anatomy of the Human Body*. 1918.

[22] O. P. Hamill, A. Marty, E. Neher, B. Sakmann, and F. J. Sigworth. Improved patch-clamp techniques for high-resolution current recording from cells and cell-free membrane patches. *Pflügers Archiv European Journal of Physiology*, 391(2):85–100, 8 1981.

[23] M. M. Hilscher, R. N. Leão, S. J. Edwards, K. E. Leão, and K. Kullander. Chrna2-Martinotti Cells Synchronize Layer 5 Type A Pyramidal Cells via Rebound Excitation. *PLOS Biology*, 15(2):e2001392, 2 2017.

[24] M. Hines, A. Davison, and E. Muller. NEURON and Python. *Frontiers in Neuroinformatics*, 3(JAN):1, 1 2009.

[25] M. L. Hines and N. T. Carnevale. NEURON: A tool for neuroscientists. *Neuroscientist*, 7(2):123–135, 4 2001.

[26] A. L. Hodgkin and A. F. Huxley. A quantitative description of membrane current and its application to conduction and excitation in nerve. *The Journal of Physiology*, 117(4):500–544, 8 1952.

[27] W. Hu, C. Tian, T. Li, M. Yang, H. Hou, and Y. Shu. Distinct contributions of Nav1.6 and Nav1.2 in action potential initiation and backpropagation. *Nature Neuroscience*, 12(8):996–1002, 8 2009.

[28] J. Isakovic, I. Dobbs-Dixon, D. Chaudhury, and D. Mitrecic. Modeling of inhomogeneous electromagnetic fields in the nervous system: a novel paradigm in understanding cell interactions, disease etiology and therapy. *Scientific Reports 2018 8:1*, 8(1):1–20, 8 2018.

[29] M. Iwamoto. Science Topics - 83.

[30] E. Kandel, editor. *Nerve Cells, Neural Circuitry, and Behavior | Principles of Neural Science, Fifth Edition | AccessNeurology | McGraw-Hill Medical*.

[31] G. M. Kapalka. Pharmacodynamics. In *Nutritional and Herbal Therapies for Children and Adolescents*, pages 47–70. Elsevier, 1 2010.

[32] P. Krishnamurthy, G. Silberberg, and A. Lansner. A Cortical Attractor Network with Martinotti Cells Driven by Facilitating Synapses. *PLOS ONE*, 7(4):e30752, 4 2012.

[33] J. D. Kropotov. Transcranial Magnetic Stimulation. In *Functional Neuromarkers for Psychiatry*, pages 281–283. Elsevier, 1 2016.

[34] Z. F. Mainen, J. Joerges, J. R. Huguenard, and T. J. Sejnowski. A model of spike initiation in neocortical pyramidal neurons. *Neuron*, 15(6):1427–1439, 1995.

[35] H. Markram, E. Muller, S. Ramaswamy, M. W. Reimann, M. Abdellah, C. A. Sanchez, A. Ailamaki, L. Alonso-Nanclares, N. Antille, S. Arsever, G. A. A. Kahou, T. K. Berger, A. Bilgili, N. Buncic, A. Chalimourda, G. Chindemi, J. D. Courcol, F. Delalondre, V. Delattre, S. Druckmann, R. Dumusc, J. Dynes, S. Eilemann, E. Gal, M. E. Gevaert, J. P. Ghobril, A. Gidon, J. W. Graham, A. Gupta, V. Haenel, E. Hay, T. Heinis, J. B. Hernando, M. Hines, L. Kanari, D. Keller, J. Kenyon, G. Khazen, Y. Kim, J. G. King, Z. Kisvarday, P. Kumbhar, S. Lasserre, J. V. Le Bé, B. R. Magalhães, A. Merchán-Pérez, J. Meystre, B. R. Morrice, J. Muller, A. Muñoz-Céspedes, S. Muralidhar, K. Muthurasa, D. Nachbaur, T. H. Newton, M. Nolte, A. Ovcharenko, J. Palacios, L. Pastor, R. Perin, R. Ranjan, I. Riachi, J. R. Rodríguez, J. L. Riquelme, C. Rössert, K. Sfyrakis, Y. Shi, J. C. Shillcock, G. Silberberg, R. Silva, F. Tauheed, M. Telefont, M. Toledo-Rodriguez, T. Tränkler, W. Van Geit, J. V. Díaz, R. Walker, Y. Wang, S. M. Zaninetta, J. Defelipe, S. L. Hill, I. Segev, and F. Schürmann. Reconstruction and Simulation of Neocortical Microcircuitry. *Cell*, 163(2):456–492, 10 2015.

[36] R. A. McDougal, T. M. Morse, T. Carnevale, L. Marenco, R. Wang, M. Migliore, P. L. Miller, G. M. Shepherd, and M. L. Hines. Twenty years of ModelDB and beyond: building essential modeling tools for the future of neuroscience, 2 2017.

[37] S. C. Murphy, L. M. Palmer, T. Nyffeler, R. M. Müri, and M. E. Larkum. Transcranial magnetic stimulation (TMS) inhibits cortical dendrites. *eLife*, 5, 3 2016.

[38] L. Palmer, M. Murayama, and M. Larkum. Inhibitory regulation of dendritic activity in vivo, 5 2012.

[39] D. P. Pelvig, H. Pakkenberg, A. K. Stark, and B. Pakkenberg. Neocortical glial cell numbers in human brains. *Neurobiology of Aging*, 29(11):1754–1762, 11 2008.

[40] M. Pospischil, M. Toledo-Rodriguez, C. Monier, Z. Piwkowska, T. Bal, Y. Frégnac, H. Markram, and A. Destexhe. Minimal Hodgkin-Huxley type models for different classes of cortical and thalamic neurons. *Biological Cybernetics*, 99(4-5):427–441, 11 2008.

[41] Queensland Brain Institute. Types of neurons - Queensland Brain Institute - University of Queensland.

[42] W. Rall. Membrane time constant of motoneurons. *Science (New York, N.Y.)*, 126(3271):454, 1957.

[43] W. Rall and G. M. Shepherd. Theoretical reconstruction of field potentials and dendrodendritic synaptic interactions in olfactory bulb. *Journal of neurophysiology*, 31(6):884–915, 1968.

[44] J. B. Ranck. Which elements are excited in electrical stimulation of mammalian central nervous system: A review, 11 1975.

[45] F. Rattay. Analysis of Models for External Stimulation of Axons. *IEEE Transactions on Biomedical Engineering*, BME-33(10):974–977, 1986.

[46] F. Rattay. Ways to approximate current-distance relations for electrically stimulated fibers. *Journal of Theoretical Biology*, 125(3):339–349, 4 1987.

[47] F. Rattay. Analysis of Models for Extracellular Fiber Stimulation. *IEEE Transactions on Biomedical Engineering*, 36(7):676–682, 1989.

[48] F. Rattay. *Electrical Nerve Stimulation: Theory, Experiments and Applications - Frank Rattay - Google Books*. Springer-Verlag Wien, 1990.

[49] F. Rattay. The basic mechanism for the electrical stimulation of the nervous system. *Neuroscience*, 89(2):335–346, 3 1999.

[50] F. Rattay, L. P. Paredes, and R. N. Leao. Strength-duration relationship for intra- versus extracellular stimulation with microelectrodes. *Neuroscience*, 214:1–13, 7 2012.

[51] J. R. Schwarz and G. Eikhof. Na currents and action potentials in rat myelinated nerve fibres at 20 and 37 degrees C. *Pflugers Archiv : European journal of physiology*, 409(6):569–577, 8 1987.

[52] J. R. Schwarz, G. Reid, and H. Bostock. Action potentials and membrane currents in the human node of Ranvier. *Pflügers Archiv 1995 430:2*, 430(2):283–292, 1995.

[53] G. Silberberg and H. Markram. Disynaptic Inhibition between Neocortical Pyramidal Cells Mediated by Martinotti Cells. *Neuron*, 53(5):735–746, 3 2007.

[54] D. A. Spronk, M. Arns, and P. B. Fitzgerald. Repetitive Transcranial Magnetic Stimulation in Depression. Protocols, Mechanisms, and New Developments. In *Neurofeedback and Neuromodulation Techniques and Applications*, pages 257–291. Elsevier Inc., 1 2011.

[55] S. Standring, editor. *Gray's Anatomy: The Anatomical Basis of Clinical Practice*. Elsevier, 42 edition, 2020.

[56] N. Sutaria. Mechanism of Action – The Chemistry of Tetrodotoxin.

[57] T. Takahashi. Diagram of synaptic transmission | Okinawa Institute of Science and Technology Graduate University OIST.

[58] Z. Turi, C. Normann, K. Domschke, and A. Vlachos. Transcranial Magnetic Stimulation in Psychiatry: Is There a Need for Electric Field Standardization? *Frontiers in Human Neuroscience*, 15, 3 2021.

[59] J. Urban-Ciecko and A. L. Barth. Somatostatin-expressing neurons in cortical networks. *Nature Reviews Neuroscience*, 17(7):401–409, 7 2016.

[60] J. Urban-Ciecko, E. E. Fanselow, and A. L. Barth. Neocortical somatostatin neurons reversibly silence excitatory transmission via GABAb receptors. *Current Biology*, 25(6):722–731, 3 2015.

[61] G. Van Rossum and F. L. Drake. *Python 3 Reference Manual*. CreateSpace, Scotts Valley, CA, 2009.

[62] M. Voigt and A. Kral. Cathodic-leading pulses are more effective than anodic-leading pulses in intracortical microstimulation of the auditory cortex Recent citations. 2019.

[63] Y. Wang, M. Toledo-Rodriguez, A. Gupta, C. Wu, G. Silberberg, J. Luo, and H. Markram. Anatomical, physiological and molecular properties of Martinotti cells in the somatosensory cortex of the juvenile rat. *Journal of Physiology*, 561(1):65–90, 11 2004.

[64] M. Y. Xu and A. H. Wong. GABAergic inhibitory neurons as therapeutic targets for cognitive impairment in schizophrenia, 5 2018.

[65] W. Yamada, C. Koch, and P. Adams. Multiple channels and calcium dynamics. *undefined*, 1989.